

**Unitarity in composite Higgs boson approaches with vector resonances**Daniele Barducci,<sup>1</sup> Haiying Cai,<sup>2</sup> Stefania De Curtis,<sup>3</sup> Felipe J. Llanes-Estrada,<sup>4</sup> and Stefano Moretti<sup>5</sup><sup>1</sup>*LAPTH, Université de Savoie, CNRS, B.P. 110, F-74941 Annecy-le-Vieux, France*<sup>2</sup>*Université de Lyon, F-69622 Lyon, France; Université Lyon 1, CNRS/IN2P3, UMR5822 IPNL, F-69622 Villeurbanne Cedex, France*<sup>3</sup>*INFN, Sezione di Firenze, Via G. Sansone 1, 50019 Sesto Fiorentino, Italy*<sup>4</sup>*Departamento de Física Teórica I, University Complutense de Madrid, 28040 Madrid, Spain*<sup>5</sup>*School of Physics and Astronomy, University of Southampton, Southampton SO17 1BJ, United Kingdom*

(Received 16 January 2015; published 18 May 2015)

We examine a simple composite Higgs model (CHM) with vector resonances in addition to the Standard Model (SM) fields in perturbation theory by using the  $K$ -matrix method to implement unitarity constraints. We find that the  $W_L W_L$  scattering amplitude has an additional scalar pole (analogous to the  $\sigma$  meson of QCD) as in generic strongly interacting extensions of the SM. The mass and width of this dynamically generated scalar resonance are large and the mass behaves contrary to the vector one, so that when the vector resonance is lighter, the scalar one is heavier, and vice versa. We also attempt an interpretation of this new resonance. Altogether, the presence of the vector state with the symmetries of the CHM improve the low-energy unitarity behavior also in the scalar-isoscalar channel.

DOI: [10.1103/PhysRevD.91.095013](https://doi.org/10.1103/PhysRevD.91.095013)

PACS numbers: 12.60.Rc, 12.60.Cn, 14.80.Va

**I. INTRODUCTION**

The recent discovery of a Higgs boson [1] has revived interest in the electroweak symmetry breaking (EWSB) sector of the Standard Model (SM) and beyond. If this Higgs boson is confirmed to have exactly the couplings expected in the SM, a renormalizable theory of the EW interactions will be a closed chapter of physics history. Nevertheless, for several reasons, the particle physics community feels that there could be further new particles beyond the newly discovered Higgs boson. It is then interesting that its reported mass, about 125 GeV, is of the same magnitude as the EW gauge bosons,  $M_W \approx 82$  GeV and  $M_Z \approx 91$  GeV, while no new particles have been seen up to 600–700 GeV. Particularly stringent are the bounds on possible further  $W'$  or  $Z'$  vector bosons and other particles coupling to  $WW$  and  $WZ$  pairs below about 1.5 TeV [2].

A natural scenario that theoretically fits this insight is that of a composite Higgs model (CHM) in which the Higgs state is a naturally light quasi-Nambu-Goldstone boson (qNGB) stemming, like the longitudinal components of the gauge bosons  $W_L$  and  $Z_L$ , from the spontaneous breaking of a higher energy symmetry [3].

While we do not really know what that symmetry might be like, Occam's razor dictates to examine first those models with the minimum number of ingredients. In the EWSB sector, this means the four Goldstone bosons that seem to be the low-energy content of the theory. A minimal such choice is the  $SO(5) \rightarrow SO(4)$  breaking, proposed in [4], that we spell out in Sec. II. A key ingredient of these models is the presence of relatively low-mass  $W'$ ,  $Z'$  vector resonances. In certain dynamical strongly coupled theories, e.g., technicolor, they correspond to spin-1

diquark condensates whereas in the minimal CHM context they simply appear as gauge bosons in the hidden symmetry  $SO(5)$ . In the cases where the vector resonance mass is relatively low and accessible at the LHC, they are prominent in the scalar-scalar scattering amplitudes that we will address.

Since our goal is to look forward to the TeV and multi-TeV region where such new vector resonances may hide, and this is high energy compared with the EW scale, we can profit from the equivalence theorem (ET) [5] between the longitudinal  $W_L$  components and the  $\pi$  qNGB's. The Lagrangian density that controls their low-energy interactions is discussed in Sec. II B.

We then dedicate Sec. III to the extraction of the scattering amplitudes among the low-energy particles in leading order (LO) chiral perturbation theory, extended by new vector resonances, which would correspond to the first accessible states [at the Large Hadron Collider (LHC)] of the CHM considered here. The amplitudes therefore include contact chiral interactions that are a polynomial in  $s$  and beyond the SM (BSM) gaugelike interactions  $\rho$ - $\pi$ - $\pi$  entering through  $t$ - and  $u$ -channel vector exchanges, with  $\rho$  representing the accessible (spin-1 gauge) resonances.<sup>1</sup> The polynomial terms imply strong interactions in

<sup>1</sup>Recently, a paper discussing the potential of characterizing the underlying CHM through  $\pi\pi$  scattering in the presence of such a  $\rho$  state has appeared [6]. Technically, we use a parametrization of the scattering amplitude that is unitary, as they do, but ours is extended to the complex  $s$ -plane and has the correct analytic structure, so the model is somewhat more sophisticated and allows one to detect, in addition to the narrow vector resonance, the scalar one, which is deep in the complex plane.

spite of the Higgs being light [7,8]. We calculate three relevant scattering processes  $\pi^i \pi^j \rightarrow \pi^k \pi^l$ ,  $\pi^i \pi^j \rightarrow hh$ , and  $\pi^i \pi^j \rightarrow \pi^3 h$  (this last one vanishes due to a cancellation between vector resonances with degenerate masses). While the  $hh \rightarrow hh$  scattering vanishes at LO since  $h$  is a singlet under the custodial  $SU(2)$  symmetry, nevertheless it will enter at the one-loop level (and in our computation, upon unitarizing the coupled-channel problem).

The amplitudes are projected over the few lowest partial waves in Sec. IV, where we check the good convergence of the expansion at low energy. While the vector channel is well behaved due to the new spin-1 resonances introduced in the CHM scenario, this is not the case for the scalar-isoscalar partial wave: we note the breakdown of unitarity by perturbation theory in the 2 TeV region for values of the parameters that are still compatible with current LHC bounds. It is well known, and continues being reinstated [9] that, generically, if the couplings of the Higgs boson do not perfectly match the SM ones, unitarity violations in perturbation theory are expected (see [10] for an exception).

A traditional way out is to restrict the analysis to those values of the parameters  $f, g_s$ , the ‘compositeness’ (energy) scale and the new gauge coupling, respectively (that couple the new vector boson(s) to the longitudinal EW gauge sector), which allow perturbative unitarity to extend to relatively high scales [11], requiring for example partial ultraviolet (UV) completion so the couplings cannot be arbitrarily strong [12].

Instead, in this paper, we focus Sec. V on a non-perturbative model treatment of the partial waves by means of the  $K$ -matrix method, irrespective of the value of the coupling. The unitarization methods start with rational instead of polynomial approximations to scattering functions and thus have no problem in incorporating strong resonant poles in the complex plane that limit the convergence of the polynomial ones. They introduce some model dependence acceptable for exploratory analysis, which can however be reduced, at an increased level of sophistication, by basing them on dispersion relations or by directly working with the latter. A generic feature that we expose in detail is that unitarity in the presence of strong interactions implies a scalar pole in the two-body scattering amplitudes.

Since there are two relevant channels with distinct amplitudes,  $\pi^i \pi^j \simeq W_L W_L$ ,  $Z_L Z_L$ , and  $\pi^4 \pi^4 \equiv hh$ , we employ a  $2 \times 2$  coupled-channel reaction matrix. Then in Sec. VI we take a preliminary look at the  $\rho\rho$  threshold region, where the approach will require to be extended to include a third channel. Since at those energies, above 2–3 TeV, the particle content of the theory typically becomes richer by a maze of new resonances, we refrain from performing an analysis beyond such energy point.

Our conclusions are wrapped up in Sec. VII.

## II. GOLDSTONE BOSONS AND NEW VECTOR FIELDS IN A TWO-SITE MODEL

### A. Particle and field content

Let us, for simplicity, refer to the minimal  $SO(5)/SO(4)$  construct of a CHM, which offers the minimum number of qNGBs filling the low-energy multiplet  $(W_L^+, W_L^-, Z_L, h) \sim \vec{\pi}^T \equiv (\pi_1, \pi_2, \pi_3, \pi_4)$ , and use it as a template to construct a typical effective Lagrangian coupling vector resonances and qNGBs. The theoretical assumption is that  $\pi_4 = h$  can be identified as the light Higgs candidate and, as it becomes a qNGB, its couplings become predictable.

A convenient framework to implement spontaneous EWSB to LO in a chiral expansion is the nonlinear sigma field formalism. The fifth “ $\sigma$ ”-like field that will acquire a high-energy vacuum expectation value (VEV) breaking the symmetry is traded for a function of  $\pi = \sqrt{\pi_1^2 + \pi_2^2 + \pi_3^2 + \pi_4^2}$ .

The exponential representation  $U = \exp(i\sqrt{2}\pi^{\hat{a}}T^{\hat{a}}/f)$  naturally exposes the multiplet transformation under the global symmetry. [The BSM generators of the coset space  $SO(5)/SO(4)$  are denoted with a hat over the adjoint index,  $T^{\hat{a}}$  with  $\hat{a} = 1, 2, 3, 4$ .] Explicitly, in terms of the qNGBs,

$$U = \begin{pmatrix} \mathbf{1}_{4 \times 4} - \frac{\vec{\pi}\vec{\pi}^T}{\pi^2} \left(1 - \cos \frac{\pi}{f}\right) & \frac{\vec{\pi}}{\pi} \sin \frac{\pi}{f} \\ -\frac{\vec{\pi}^T}{\pi} \sin \frac{\pi}{f} & \cos \frac{\pi}{f} \end{pmatrix}. \quad (1)$$

Although we will not work with transverse gauge bosons in this contribution, soon setting their coupling to vanish,  $g_0 = 0$ , let us momentarily keep the covariant gauge derivative for completeness,

$$D_\mu = \partial_\mu - ig_0 A_\mu^a T^a. \quad (2)$$

We will work with a so-called “two-site model,” where there are two sets of vector fields coupled to qNGBs. The fields of the first site are the elementary gauge fields  $A_\mu$  with

$$A_\mu = W_\mu^a T_L^a + B_\mu \delta^{3a} T_R^a, \quad (3)$$

where  $T_L^a, T_R^a$ ,  $a = 1, 2, 3$  are the respective generators of  $SU(2)_L$  and  $SU(2)_R$ . The  $SU(2) \times SU(2) \simeq SO(4)$  symmetry remaining at this site is spontaneously broken to the custodial  $SU(2)$  symmetry of the SM.

At the second, higher-energy site, there are additional vector fields

$$\rho_\mu = \rho_{L,\mu}^a T_L^a + \rho_{R,\mu}^a T_R^a + a_\mu^{\hat{a}} T^{\hat{a}}. \quad (4)$$

The  $SO(5)/SO(4)$  coset gauge resonances are  $a_\mu^{\hat{a}}$  and the  $\rho_{L/R,\mu}^a$  are those associated to  $SU(2)_{L,R}$  (we will refer to them simply as vector resonances). They could be detected

by means of the Drell-Yan or di-boson processes [13–15], since they are expected to couple to two fermions in an  $s$ -wave.<sup>2</sup> But here we will focus on their couplings to two vector bosons intervening in (longitudinal) gauge boson scattering.

We may explicitly spell out the matrix representation of Eq. (4) as

$$i\rho_\mu^A T^A = \begin{pmatrix} \frac{1}{2}e^{ijk}(\rho_{L,\mu}^k + \rho_{R,\mu}^k) & \frac{1}{2}(\rho_{L,\mu}^i - \rho_{R,\mu}^i) & \frac{1}{\sqrt{2}}a_\mu^{\hat{i}} \\ -\frac{1}{2}(\rho_{L,\mu}^j - \rho_{R,\mu}^j) & 0 & \frac{1}{\sqrt{2}}a_\mu^{\hat{j}} \\ -\frac{1}{\sqrt{2}}a_\mu^{\hat{k}} & -\frac{1}{\sqrt{2}}a_\mu^{\hat{l}} & 0 \end{pmatrix}. \quad (5)$$

In the unitary gauge, at low energy and after EWSB has occurred, one can set  $\pi_1 = \pi_2 = \pi_3 = 0$ , since they provide the  $W_L$  and  $Z_L$  components. At high energy it is more convenient to work with the Goldstone fields and extract from them the  $W_L W_L$  scattering amplitude via the ET.

We thus employ all these pionlike fields and group them in a tensor parametrization

$$\Pi = \sqrt{2}\pi^{\hat{a}} T^{\hat{a}} = -i \begin{pmatrix} 0_{4 \times 4} & \vec{\pi} \\ -\vec{\pi}^T & 0 \end{pmatrix} \quad (6)$$

that is useful to construct couplings to the vector resonances.

The unitary representation in Eq. (1) may be expressed as a product of two matrices of fields, one at each site,  $U = \Omega_1 \cdot \Omega_2$ . These two matrices  $\Omega_n$ ,  $n = 1, 2$ , are constructed from the  $\Pi$  tensor in Eq. (6) by the expressions

$$\Omega_n = 1 + i \frac{s_n}{\pi} \Pi + \frac{c_n - 1}{\pi^2} \Pi^2, \quad (7)$$

$$s_n = \sin(f\pi/f_n^2), \quad c_n = \cos(f\pi/f_n^2),$$

where

$$f^2 = f_1^2 f_2^2 / (f_1^2 + f_2^2), \quad (8)$$

with  $f_{1,2}$  being the ‘‘pion decay constants’’ associated to each of the two sites respectively.

The larger symmetry is spontaneously broken at the second site  $SO(5)_2 \rightarrow SO(4)_2$  by a field  $\phi_0^T = (0, 0, 0, 0, 1)$  that acquires a VEV. The  $SO(5)$  matrix  $\Omega_2$  can be used to arbitrarily orient the direction of symmetry breaking,  $\Phi_2 = \Omega_2 \phi_0$ , and this second-site field is then calculated using Eqs. (6) and (8) to yield

<sup>2</sup>A bound on their mass can be derived from LHC run-I data by rescaling the limits from di-lepton [16] and di-boson [17] searches. It results to be around 2 TeV depending on the choice of  $f$  and  $g_s$ , the coupling strengths. Following the extrapolation procedure proposed in [18], this bound can be pushed up to 4 (5) TeV by LHC-14 (HL-LHC) data.

$$\Phi_2^T = \frac{1}{\pi} \sin(f\pi/f_2^2) (\pi_1, \pi_2, \pi_3, \pi_4, \pi \cot(f\pi/f_2^2)). \quad (9)$$

## B. Effective Lagrangian

The coupling between the pion fields and the vector fields active at each of the two theory sites is determined by a minimum-coupling principle introducing covariant derivatives,

$$D_\mu \Omega_1 = \partial_\mu \Omega_1 - ig_0 A_\mu \Omega_1 + ig_s \Omega_1 \rho_\mu, \quad (10)$$

$$D_\mu \Phi_2 = \partial_\mu \Phi_2 - ig_s \rho_\mu \Phi_2,$$

where  $g_s$  is the coupling strength associated with the new resonances.

Likewise, we introduce a field-strength tensor for the new vector fields that allows the construction of a gauge-invariant Lagrangian density (in the philosophy that there is a hidden gauge symmetry) as  $\rho_{\mu\nu} = \partial_\mu \rho_\nu - \partial_\nu \rho_\mu - ig_s [\rho_\mu, \rho_\nu]$ . In our application to ‘‘low-energy’’  $W_L W_L$  scattering, the  $\rho$  self-interaction is considered in the inelastic scattering  $\pi\pi \rightarrow \rho\rho$  at a higher energy scale, where the trilinear vertex  $\rho\rho\rho$  will enter into the  $s$ -channel of this process.

The resulting  $\sigma$ -model Lagrangian is then

$$\mathcal{L}_{2\text{-site}} = \frac{f_1^2}{4} \text{Tr}(D_\mu \Omega_1)^\dagger D_\mu \Omega_1 + \frac{f_2^2}{2} (D_\mu \Phi_2)^T D_\mu \Phi_2 - \frac{1}{4} \text{Tr} \rho_{\mu\nu} \rho^{\mu\nu}. \quad (11)$$

We should immediately acknowledge that the effective Lagrangian in Eq. (11) does not contain the most possible general interactions. First, it is built under the principle of a hidden gauge symmetry (using gauge theory as a template for the interaction of the new vector fields, when it is clear that new resonances may or may not be gauge bosons themselves). Second, higher derivative, nonrenormalizable counterterms should be added if further new physics lied at yet higher energy scales, though only relevant operators remain at low energy. Additionally, we could mix the fields of the first site and the second site into a ‘‘theory-space’’ nonlocal term [19–21] which is allowed by the symmetries. This would be accomplished by defining  $\Phi = \Omega_1 \Omega_2 \phi_0$  or

$$\Phi^T = \frac{1}{\pi} \sin(\pi/f) (\pi_1, \pi_2, \pi_3, \pi_4, \pi \cot(\pi/f)) \quad (12)$$

in analogy with Eq. (9), which provides the additional two-derivative term

$$\mathcal{L}^{(2)} = \frac{f_0^2}{2} (D^\mu \Phi)^T D_\mu \Phi. \quad (13)$$

In the rest of this paper we will not pursue Eq. (13) further but rather limit ourselves to the low-energy

consequences of Eq. (11) in the presence of relatively strongly coupled new vector fields. This allows us to neglect the transverse gauge bosons  $W_T$ ,  $Z_T$ , turning off the EW interaction, i.e.,  $g_0 \rightarrow 0$ .

We then consider  $W_L W_L$  (through the ET, pion-pion) scattering. To reveal the  $g_s$  content of Eq. (11) we expand the two  $\Omega$  fields, yielding

$$\Omega_1 = \begin{pmatrix} 1_{4 \times 4} - \frac{f^2}{2f_1^4} \vec{\pi} \vec{\pi}^T & \frac{f}{f_1^2} \vec{\pi} \left(1 - \frac{f^2}{6f_1^4} \pi^2\right) \\ -\frac{f}{f_1^2} \vec{\pi}^T \left(1 - \frac{f^2}{6f_1^4} \pi^2\right) & 1 - \frac{f^2}{2f_1^4} \pi^2 \end{pmatrix} + \mathcal{O}(\pi^4), \quad (14)$$

$$\Omega_2 = \begin{pmatrix} 1_{4 \times 4} - \frac{f^2}{2f_2^4} \vec{\pi} \vec{\pi}^T & \frac{f}{f_2^2} \vec{\pi} \left(1 - \frac{f^2}{6f_2^4} \pi^2\right) \\ -\frac{f}{f_2^2} \vec{\pi}^T \left(1 - \frac{f^2}{6f_2^4} \pi^2\right) & 1 - \frac{f^2}{2f_2^4} \pi^2 \end{pmatrix} + \mathcal{O}(\pi^4). \quad (15)$$

In the unitary gauge both the first and second terms in the Lagrangian density  $\mathcal{L}_{2\text{-site}}$  of Eq. (11) contribute to the vertex  $\rho\pi\pi$ . In particular, the  $L$  and  $R$  vector couplings are unequal and separately listed. On the contrary, the coset resonances  $\hat{a}_\mu$  defined in (4), have only a small coupling to  $\pi^a$  induced after EWSB [19].

From the first term in  $\mathcal{L}_{2\text{-site}}$  we obtain, with  $i, j, k$ , taking the values 1,2,3,

$$\mathcal{L}_{\rho_L \pi \pi}^{(1)} = \frac{f^2 g_s}{4f_1^2} [\epsilon^{ijk} \pi^i \partial_\mu \pi^j \rho_{L\mu}^k + (\pi^k \partial_\mu \pi^4 - \pi^4 \partial_\mu \pi^k) \rho_{L\mu}^k], \quad (16)$$

$$\mathcal{L}_{\rho_R \pi \pi}^{(1)} = \frac{f^2 g_s}{4f_1^2} [\epsilon^{ijk} \pi^i \partial_\mu \pi^j \rho_{R\mu}^k - (\pi^k \partial_\mu \pi^4 - \pi^4 \partial_\mu \pi^k) \rho_{R\mu}^k], \quad (17)$$

and, from the second term in  $\mathcal{L}_{2\text{-site}}$ ,

$$\mathcal{L}_{\rho_L \pi \pi}^{(2)} = \frac{f^2 g_s}{2f_2^2} [\epsilon^{ijk} \pi^i \partial_\mu \pi^j \rho_{L\mu}^k + (\pi^k \partial_\mu \pi^4 - \pi^4 \partial_\mu \pi^k) \rho_{L\mu}^k], \quad (18)$$

$$\mathcal{L}_{\rho_R \pi \pi}^{(2)} = \frac{f^2 g_s}{2f_2^2} [\epsilon^{ijk} \pi^i \partial_\mu \pi^j \rho_{R\mu}^k - (\pi^k \partial_\mu \pi^4 - \pi^4 \partial_\mu \pi^k) \rho_{R\mu}^k], \quad (19)$$

while the  $4\pi$  vertices, with indices  $a, b = 1, 2, 3, 4$ , are collected as

$$\begin{aligned} & \frac{f_1^2}{4} \text{Tr}(\partial_\mu \Omega_1)^\dagger \partial_\mu \Omega_1 + \frac{f}{2} (\partial_\mu \Phi_2)^\dagger \partial_\mu \Phi_2 \\ & \Rightarrow \mathcal{L}_{4\pi} = \frac{f^4}{24f_1^6} [(\pi^a \partial_\mu \pi^a)^2 - (\pi^a \partial_\mu \pi^b)^2] \\ & + \frac{f^4}{6f_2^6} [(\pi^a \partial_\mu \pi^a)^2 - (\pi^a \partial_\mu \pi^b)^2]. \end{aligned} \quad (20)$$

The resulting effective interaction Lagrangian that combines Eq. (16) through (20) can be employed in an energy range that is sufficiently above  $2m_W \simeq 2m_h$  so that the ET applies and SM couplings are weaker than BSM couplings. Since  $\rho$  pair production is not described by the terms that we have kept in the  $\pi\pi \rightarrow \pi\pi$  amplitudes, we also need to satisfy  $\sqrt{s} < 2m_\rho$ , and we expect this scale to be similar to that intrinsic to the chiral expansion  $4\pi f$ , above which further derivative terms should also be included in the  $\pi\pi$  amplitude. Thus, the model Lagrangian can be of use in the energy range (0.4,3) TeV for  $m_\rho \simeq 2$  TeV. At the LHC, the low-energy end of this range is accessible and the polarization combination  $W_L W_L$  can be activated.

The independent BSM parameters in the above Lagrangian density are three, namely  $f_1$ ,  $f_2$  and  $g_s$ , and they are related by the mass relations

$$m_{\rho_L}^2 = m_{\rho_R}^2 = g_s^2 f_1^2 / 2, \quad (21)$$

$$m_a^2 = g_s^2 (f_1^2 + f_2^2) / 2, \quad (22)$$

which hold true before the acquisition of a VEV by the Higgs field  $h$  upon EWSB. Equation (21) is the so-called KSFR relation [22]. This is not generally valid for BSM theories with an additional vector resonance but it is a consequence of the high symmetry imposed when the vector resonance is coupled to the Goldstone bosons as a gauge boson. Therefore, Eq. (21) is a prediction of the theory in Eq. (11). Notice also that the degeneration between  $\rho_L$  and  $\rho_R$  holds for  $g_0 = 0$ . Since we work in this approximation, we will take  $m_{\rho_L} = m_{\rho_R} \equiv m_\rho$ .

### III. SCATTERING AMPLITUDES

#### A. Tree-level amplitudes

We now extract the  $\pi^i \pi^j \rightarrow \pi^k \pi^l$  scattering amplitude according to the Feynman diagrams in Fig. 1. This we denote as  $A^{(\pi\pi \rightarrow \pi\pi)}$  or  $A$  for short. Likewise we can obtain the inelastic  $M^{(\pi\pi \rightarrow hh)}$ ,  $N^{(\pi\pi \rightarrow \pi h)}$ , as well as the elastic  $T^{(hh \rightarrow hh)}$  amplitudes, also shortened to  $M$ ,  $N$  and  $T$ , respectively. The elastic  $hh$  scattering amplitude  $T$  is not readily accessible at the LHC, since Higgs production rates are quite small and the final state reconstruction is quite poor, so that the final state  $hh$  is rather unlikely and the initial state  $hh$  does not abound either (owing to small Yukawa couplings to the proton content). Additionally, in the considered CHM setup the  $hh$  elastic amplitude

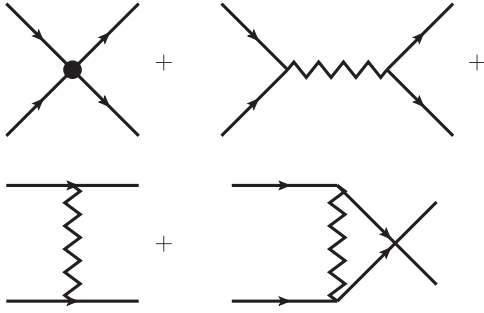


FIG. 1. Feynman diagrams that produce the tree-level amplitudes for pion ( $W_L$ ) scattering in the energy range  $2m_{W,h} \ll \sqrt{s} \ll 4\pi f \sim$  several TeV.

vanishes in leading order in  $s$ , so that the BSM low-energy production must proceed from the  $W_L W_L$  channel in the CHM. (Nevertheless, the virtual re-scattering  $W_L W_L \rightarrow hh \rightarrow W_L W_L$  can bring this dynamics into the visible  $W_L W_L$  sector and some experimental information might be provided by the LHC, though a CLIC-type machine would be needed for a better study [23]).

Concentrating now on the elastic  $\pi\pi$  amplitude, we note the following well-known isospin structure:

$$A(\pi^i \pi^j \rightarrow \pi^k \pi^l) = A(s, t, u) \delta^{ij} \delta^{kl} + A(t, s, u) \delta^{ik} \delta^{jl} + A(u, t, s) \delta^{il} \delta^{jk}. \quad (23)$$

Standard calculation for the “two-site” model, considering the exchanges of  $\rho_{L,R}$  (see [24] for a related work in an other construction), with  $m_{\rho_{L,R}} = m_\rho$  and neglecting terms  $O(m_h^2/s)$ , leads to

$$A(s, t, u) = \left( \frac{f^4}{4f_1^6} + \frac{f^4}{f_2^6} \right) s - \frac{g_s^2}{2} \left( \frac{f^2}{2f_1^2} + \frac{f^2}{f_2^2} \right)^2 \left[ \frac{s-u}{t-m_\rho^2} + \frac{s-t}{u-m_\rho^2} \right]. \quad (24)$$

Notice that  $\rho_L$  and  $\rho_R$  contribute to this amplitude with equal amounts, because the different sign in the Lagrangian densities of Eqs. (16) and (18) affects only vertices with  $\pi^4 = h$  that do not appear in tree-level  $\pi^i \pi^j \rightarrow \rho_{L,R} \rightarrow \pi^k \pi^l$ .

Since, in virtue of the co-called BRST identities [25], the interacting bosons are effectively spinless, an efficient low-energy representation of the amplitude is obtained in terms of a few partial-wave projections. We first project to definite isospin

$$A_0(s, t, u) = 3A(s, t, u) + A(t, s, u) + A(u, t, s), \quad (25)$$

$$A_1(s, t, u) = A(t, s, u) - A(u, t, s), \quad (26)$$

$$A_2(s, t, u) = A(t, s, u) + A(u, t, s), \quad (27)$$

and then to definite  $J = l$ ,

$$a_J^l(s) = \frac{1}{64\pi} \int_{-1}^{+1} d \cos \theta P_J(\cos \theta) A_l(s, t(s, \cos \theta)), \quad (28)$$

with  $\cos \theta = 1 + 2t/s$ .

The resulting partial waves consist of two parts: a power expansion, coming from the purely  $\pi\pi$  Lagrangian density, and terms due to  $\rho$  exchange (at the lowest end of the  $\sqrt{s}$  interval these could also be projected into low-energy derivative terms, but since we are exploring the model with additional vector resonances, we keep the  $\rho$  propagator explicitly).

Next, let us quote the inelastic scattering amplitude, which has weak isospin 0 by necessity,  $M(\pi^i \pi^j \rightarrow hh) = M(s, t, u) \delta^{ij}$ ,

$$M(s, t, u) = \left( \frac{f^4}{4f_1^6} + \frac{f^4}{f_2^6} \right) \left( s - \frac{2}{3} m_h^2 \right) - \frac{g_s^2}{2} \left( \frac{f^2}{2f_1^2} + \frac{f^2}{f_2^2} \right)^2 \left( \frac{s-u}{t-m_\rho^2} + \frac{s-t}{u-m_\rho^2} \right) - \frac{g_s^2}{2} \left( \frac{f^2}{2f_1^2} + \frac{f^2}{f_2^2} \right)^2 \frac{m_h^4}{m_\rho^2} \left( \frac{1}{t-m_\rho^2} + \frac{1}{u-m_\rho^2} \right). \quad (29)$$

Here the charged resonances  $\rho_{L,R}^\pm$ , which are degenerate with the neutral ones before EWSB and in the  $g_0 \rightarrow 0$  limit, are exchanged in the  $t$  and  $u$  channel. This amplitude entails probability leak from the entry  $W_L W_L$  channel to the (rather uncommon)  $hh$  one. If, surprisingly, a large number of  $hh$  events were visible at the LHC, this would point out to strong dynamics coupling this channel to  $W_L W_L$ . Notice that, for values of  $m_\rho$  around 2 TeV or larger,  $m_h$  and thus the last term in Eq. (29) are negligible and  $M(s, t, u) \approx A(s, t, u)$ . Finally, let us consider the inelastic scattering amplitude  $N(\pi^i \pi^j \rightarrow \pi^k h) = N(s, t, u) \delta^{ij} \delta^{k3}$ ,

$$N(s, t, u) = \frac{g_s^2}{2} \left( \frac{f^2}{2f_1^2} + \frac{f^2}{f_2^2} \right)^2 \left( \frac{u-t}{s-m_{\rho_L}^2} + \frac{s-u}{t-m_{\rho_L}^2} + \frac{s-t}{u-m_{\rho_L}^2} \right) - (L \rightarrow R). \quad (30)$$

Note that, since we have  $m_{\rho_L} = m_{\rho_R}$ , in the limit  $g_0/g_s \rightarrow 0$ , this amplitude vanishes in this simple CHM. The reason for this is twofold. First, the  $\rho_L$  and  $\rho_R$  exchange contributions to the amplitude are equal and with opposite sign, so they cancel due to the different sign in the Lagrangian densities of Eqs. (16) and (18) which affects vertices with  $\pi^4 = h$ . Second, the chiral pion interactions for this process are known to start at order  $p^6$  (we have only the low-energy  $p^2$  terms plus those coming from vector boson exchange) and they require a violation of discrete

parities, as discussed in [12]. We thus ignore this channel in the following.

### B. Parameters

To shorten notation in Eqs. (24) and (29), and in view of the standard factor in the partial wave projection in Eq. (28), it is useful to employ two constants  $K_1$  and  $K_2$  defined as

$$\begin{aligned} K_1 &= \frac{1}{16\pi} \left( \frac{f^4}{4f_1^6} + \frac{f^4}{f_2^2} \right), \\ K_2 &= \frac{g_s^2}{16\pi} \left( \frac{f^2}{2f_1^2} + \frac{f^2}{f_2^2} \right)^2 \end{aligned} \quad (31)$$

(notice that  $K_1$  is dimensionful).

For the minimal CHM to have only the  $\rho_{L,R}$  and no further resonances in the low-energy region, we need to split up the coset resonances: this is achieved by requiring  $f_2 \rightarrow \infty$ . This simplifies Eq. (31), since from Eq. (8)  $f \rightarrow f_1$ , to read

$$K_1 = \frac{1}{32\pi} \frac{1}{2f^2}, \quad (32)$$

$$K_2 = \frac{g_s^2}{64\pi} = \frac{1}{32\pi} \frac{m_\rho^2}{f^2}. \quad (33)$$

In this limit, the model has only two parameters,  $f$  and  $g_s$  [or equivalently  $f$  and  $m_\rho$  after using Eq. (21)], which can be immediately obtained once the amplitudes (functions of  $K_1$  and  $K_2$ ) become known, by solving  $g_s = 8\sqrt{\pi K_2}$  and  $f = \frac{1}{8\sqrt{\pi K_1}}$ . Nevertheless, there is a third parameter, necessary to regulate the pole of the vector resonance,  $\Gamma_\rho$ , which is generally independent of the other two,  $f$  and  $m_\rho$ .

Because of Eq. (38) below,  $K_2$  could be traded for the common partial  $\pi\pi$  widths of the new vector particles  $\Gamma_{\rho\pi\pi}$  [in fact  $\rho_{L,R}$  have the same mass in the degenerate limit and the same couplings to  $\pi\pi$  as it is clear from Eqs. (16)–(18)]. Note that  $\Gamma_\rho \simeq \Gamma_{\rho\pi\pi}$  if there were no extra strongly coupled fermions to which the vector particles could have a sizable decay amplitude, for example, because they would be as heavy as or heavier than the  $\rho$  itself. But, if instead there were such fermions, what would appear in the propagators is the total width  $\Gamma_\rho$  as opposed to the partial  $\pi\pi$  width in Eq. (38) [15]. It is also true that in CHMs, the top quark has a composite component (via the partial compositeness mechanism) and, as a consequence, it is sizably coupled to the new vector resonances leading to a non-negligible  $t\bar{t}$  decay channel. Thus we have  $\Gamma_\rho$  as a free parameter of our analysis but, for moderate values of the order a few percent, it does not make a large difference except in the vector-isovector channel itself (of course, in other channels the

TABLE I. Dependent and independent parameters in the two scenarios considered in our numeric computations.  $K_1$ ,  $K_2$ ,  $m_\rho$  and  $g_s$  directly appear in our amplitudes and could thus be reconstructed from experiment in principle.

Parameter	Scenario 1	Scenario 2
	( $\hat{a}_\mu$ decoupled)	(complete 4DCHM)
$f_1$	$= f$	$= \sqrt{2}m_\rho/g_s$
$f_2$	$\infty$	$\frac{1}{f_2^2} = \frac{1}{f^2} - \frac{1}{f_1^2}$
$f$	Independent variable	Independent variable
$m_\rho$	Independent variable	Independent variable
$g_s$	$= \sqrt{2}m_\rho/f$	Independent variable
$\Gamma_\rho$	Independent variable	Independent variable
$K_1$	$= \frac{1}{16\pi} \frac{1}{4f^2}$	$K_1(f, m_\rho, g_s)$
$K_2$	$= \frac{1}{16\pi} \frac{m_\rho^2}{2f^2}$	$K_2(f, m_\rho, g_s)$

vector state is exchanged in  $t$  and  $u$  diagrams, where its width just slightly modifies low-energy potentials).

In our plots, both  $f$  and  $m_\rho$  will be taken as relatively small, for which the effects we are describing are relevant at the LHC run II but are not yet discarded by LHC run-I studies. Particularly on  $f$  there are somewhat more stringent bounds from LEP, but these are based on loop computations that are to be taken with a grain of salt because they (currently) cut off the virtual effects of any new high-energy physics.

We contrast this three-parameter scenario with a more complete one, e.g., the four-dimensional CHM (4DCHM) of Ref. [19], with a finite  $f_2$  corresponding to nondecoupled coset resonances but sufficiently heavy to be undetected by the LHC. Even if the coset resonances are only smoothly coupled to  $\pi\pi$  so that we can neglect their contribution in the tree level amplitudes, their presence is indirectly manifest by the dependence of  $K_1$  and  $K_2$  on  $f_2$ . In this second scenario there are up to four free parameters that can be taken as  $f$ ,  $g_s$ ,  $m_\rho$  and  $\Gamma_\rho$ .

With one or the other scenario we should have enough flexibility to describe in an effective way many models that just have vector resonances at low energy in addition to the already known EWSB sector including a SM-like Higgs state. For example, the Higgs-like boson under study would be a dilaton (so that there are further strong interactions in the EWSB sector) and there is an additional vector boson. Another possibility would be that the B-L seemingly accidental symmetry was actually a gauge symmetry, which would bring about an additional vector boson but without the relation in Eq. (8).

For convenience, the parameter content for the two scenarios is summarized in Table I.

### IV. ELASTIC PARTIAL WAVES

We now quote the lowest nonvanishing partial waves for each isospin channel from Eq. (28). These are

$$a_0^0(s) = K_1 s + K_2 \left[ \left( \frac{m_\rho^2}{s} + 2 \right) \log \left( 1 + \frac{s}{m_\rho^2} \right) - 1 \right], \quad (34)$$

$$a_1^1(s) = \frac{K_1}{6} s + \frac{K_2}{6s^2(m_\rho^2 - s)} \left[ -s(6m_\rho^4 + 6m_\rho^2 s - 13s^2) + 3(2m_\rho^6 + 3m_\rho^4 s - 3m_\rho^2 s^2 - 2s^3) \log \left( 1 + \frac{s}{m_\rho^2} \right) \right] \quad (35)$$

and

$$a_2^2(s) = \frac{-K_1}{2} s - \frac{K_2}{2} \left[ \left( \frac{m_\rho^2}{s} + 2 \right) \log \left( 1 + \frac{s}{m_\rho^2} \right) - 1 \right] \quad (36)$$

[the first and third ones satisfy  $a_0^2(s) = -\frac{1}{2}a_0^0(s)$ ]. These are the lowest-order partial wave projections in each isospin channel: higher ones are suppressed by an additional power of  $s$ . For example, in the isoscalar channel, the tensor ( $l = 2$ ) partial wave starts as

$$a_2^0(s) = \frac{K_2}{s^2} \left( \frac{m_\rho^2}{s} + 2 \right) \left[ -3s(2m_\rho^2 + s) + (6m_\rho^4 + 6m_\rho^2 s + s^2) \log \left( 1 + \frac{s}{m_\rho^2} \right) \right], \quad (37)$$

i.e., without the linear term  $\propto K_1 s$ .

Let us delve in the amplitudes for a few lines. First, we notice that the isotensor partial wave  $a_2^0$  is repulsive at low energy, as Eq. (36) has an explicit negative sign, while the other two channels are attractive. Thus, if a doubly charged resonance couples  $W^+ W^+$ , this means that this partial wave probably changes sign (to avoid violating Wigner's causality bound), driven by higher order chiral terms, and the convergence of the series will be very poor.

Our second observation is that, naturally, the vector-isovector partial wave in Eq. (35) presents a simple pole at  $s = m_\rho^2$ . Of course, this singularity is just a feature of perturbation theory blindly applied: if we resum the  $\pi\pi$  bubble insertions in the  $\rho$  propagator, the BSM-vector width  $\Gamma_\rho$  naturally regulates the denominator. Then, one should substitute  $\frac{1}{m_\rho^2 - s}$  by  $\frac{1}{(m_\rho - i\Gamma_\rho/2)^2 - s}$ . This isovector partial wave is the only one that acquires an imaginary part at this stage; the others remain real and are thus in violation of unitarity, which is only satisfied in perturbation theory by proceeding to the next order. Again, in the case in which the fermion decay channels are suppressed, the width is dominated by the partial width  $\Gamma_{\rho\pi\pi}$ , otherwise it is an independent parameter.

A straightforward calculation yields

$$\Gamma_{\rho\pi\pi} = m_\rho \frac{K_2}{6}, \quad (38)$$

an equation that provides a beautiful interpretation of the chiral constant  $K_2$  in terms of  $\Gamma_{\rho\pi\pi}/m_\rho$  which simply becomes

$$\Gamma_{\rho\pi\pi} = \frac{m_\rho^3}{192\pi f^2} \quad (39)$$

in scenario 1, where one can eliminate  $g_s$ .

An important observation is that the contribution of the BSM vector resonance to Eq. (34) is positive. For  $s < m_\rho^2$ , in the low-energy regime, the factor

$$\left[ \left( \frac{m_\rho^2}{s} + 2 \right) \log \left( 1 + \frac{s}{m_\rho^2} \right) - 1 \right] \sim \frac{3s}{2m_\rho^2} > 0. \quad (40)$$

Thus, at low energy, Eq. (34) becomes

$$a_0^0(s) = \left( K_1 + \frac{3K_2}{2m_\rho^2} \right) s. \quad (41)$$

The ratio of the two terms in this expression happens to be, for  $m_{\hat{a}}$  not too far from  $m_\rho$  (else we are in scenario 1),  $3(m_{\hat{a}}^2 - m_\rho^2)/(2m_\rho^2)$ . So, if  $m_{\hat{a}} > m_\rho$  and the two states are not closely degenerate (which would invalidate our treatment anyway because an explicit  $\hat{a}$  resonance would have to enter the amplitudes), both terms contribute to the low-energy theorem.

By using the explicit expressions for  $K_1$  and  $K_2$  in Eq. (31) plus  $m_\rho$  in Eq. (21), we get the low-energy ( $s < m_\rho^2$ ) behavior for the scalar partial wave,

$$a_0^0(s) \simeq \frac{s}{16\pi f^2} \frac{f^6}{f_1^6} \left[ \left( \frac{1}{4} + \frac{f_1^6}{f_2^6} \right) + \frac{3}{4} \left( 1 + 2 \frac{f_1^2}{f_2^2} \right)^2 \right] \simeq \frac{s}{16\pi f^2}, \quad (42)$$

with the first contribution from the four-pion contact terms and the second from the  $\rho$ -exchange terms. These two contributions sum up to the expected low-energy result for  $a_0^0$  being regulated only by the symmetry breaking scale  $f$ . It is easy to check it in scenario 1 ( $f_2 \rightarrow \infty, f_1 = f$ ), but it holds true for any choice of  $f_2$  which satisfies the relation in Eq. (8). This result does not depend on the  $\rho$  mass or coupling, so at this order the scale of unitarity saturation is totally controlled by  $f$ . Actually, at the next order there is some amelioration (the unitarity scale is pushed higher) because the logarithm in Eq. (40) is an alternating series and the next term is negative, slightly reducing  $f$ . This happens at order  $s^2/m_\rho^4$ ,

$$a_0^0 \simeq \frac{s}{16\pi f^2} - s^2 \left( \frac{2K_2}{3m_\rho^4} \right). \quad (43)$$

### A. Matching to low-energy effective theory

From the LHC run-I data other investigators have extracted some bounds on the low-energy coefficients of operators extending the SM in the language of effective theory that is being used profusely, especially in the nonlinear representation of the sigma model [26–29].

We can profit from this approach to reduce the parameter space that needs to be explored. Taking again the low-energy limit of our expression for  $a_0^0$  in Eq. (43), we can identify the leading term in the commonly used expression [30]

$$a_0^0 \simeq \frac{1}{16\pi v^2} (1 - a^2)s, \quad (44)$$

where currently  $a \in (0.7, 1.3)$  is not excluded by the LHC run I [31] (in the weakly coupled SM,  $a = 1$  and this strong amplitude vanishes). Since the  $s$  coefficient is positive, the relevant bound for us is the lower one,  $a \geq 0.7$ .

By comparing with Eq. (43), in our CHM  $a^2 = 1 - v^2/f^2$ . For large  $m_\rho$  so that  $s^2/m_\rho^4$  may be neglected, we have

$$f \geq 350 \text{ GeV}. \quad (45)$$

[If  $m_\rho$  is kept finite and the next-to-leading-order (NLO) term in Eq. (43) is not negligible, then the bound is a little bit less stringent: for example, for  $s = m_\rho^2/2$  the bound is lowered to  $\sim 320$  GeV.] Since one naturally expects  $f > v$  we will explore this range of values of  $f$  in the following. We do not employ precision EW constraints here since they are contingent on what new physics enters through loop corrections [31].

The comparison with the SM in the linear representation is not direct, so we discuss it very briefly. Bounds are often given for the coupling ratio  $k_V^2 = \frac{\Gamma_{h \rightarrow VV}}{\Gamma_{SM}^{h \rightarrow VV}}$ . Currently, CMS [32] quotes in its run-I legacy paper a  $2\sigma$  lower bound on  $k_V$  of about 0.87 based on its complex global analysis. The direct measurement for  $h \rightarrow VV$  is less constraining and  $k_V \sim 0.76$  would remain possible: to exclude it one would have to rely on the pull towards higher  $k_V$  of  $h \rightarrow \tau\tau$ , a notoriously difficult channel. Moreover, if several degrees of freedom are allowed to vary simultaneously from their SM values, the bound even relaxes to  $k_V > 0.66$  (still at  $2\sigma$  or 95% confidence level).

The  $h \rightarrow VV$  decay amplitude in the linear representation of the symmetry breaking (the usual SM) is proportional to  $\frac{M_V^2}{v}$  whereas a typical one in the low-energy limit of a CHM is  $\sim a \frac{P_1 P_2}{v} = \frac{P_1 P_2}{f}$ . This would suggest  $a \sim k_V$ , so that  $f = 350$  GeV, giving  $a = v/f = 0.7 \sim k_V$ , would be the extreme acceptable case in view of the bounds just quoted. But this comparison is to be taken with a grain of salt: the degrees of freedom in the two theories are different. Whereas the SM bounds are given in terms of the gauge

bosons themselves, the effective Lagrangian and CHM are most transparently formulated (as we have done) in terms of the Goldstone bosons. They coincide only at  $E \gg M_W$  (say above 500 GeV, the region of our interest). But the experimental bounds are taken with the Higgs on shell, that is,  $E \sim M_W$  and thus, the bounds from  $k_V$  are not strict.

Next we compare the inelastic amplitude  $M_0^0$  for  $\pi\pi|_{I=0} \rightarrow hh$  between the actual CHM and the low-energy effective theory. For this, let us quickly reorder the amplitude in Eq. (29) to expose it as a power series in  $m_h$ , from which we will keep only the zeroth order term since we are also neglecting  $M_W$  and  $M_Z$  that are of the same order in any sensible counting,

$$\begin{aligned} M(s, t, u) = & 16\pi K_1 s - 8\pi K_2 \left( \frac{s-u}{t-m_\rho^2} + \frac{s-t}{u-m_\rho^2} \right) \\ & - \frac{32\pi}{3} K_1 m_h^2 \\ & - 8\pi K_2 \frac{m_h^4}{m_\rho^2} \left( \frac{1}{t-m_\rho^2} + \frac{1}{u-m_\rho^2} \right). \end{aligned}$$

In the massless limit we immediately note the equality with the elastic amplitude  $M(m_h = 0) = A(s, t, u)$ . To obtain the isospin-zero projection we note that the Clebsch-Gordan coefficients rotating  $|\pi^a \pi^b\rangle$  to  $|\pi\pi\rangle_{I=0}$  bring in factors of  $1/\sqrt{3}$  so that

$$\begin{aligned} M_0 &= \frac{1}{\sqrt{3}} \sum_a M(\pi^a \pi^a \rightarrow hh) \\ &= \sqrt{3} M. \end{aligned} \quad (46)$$

Then the scalar partial wave projection of that cross-channel amplitude  $M_0$  becomes

$$M_0^0 = \frac{1}{64\pi} \int_{-1}^1 dx M_0(s, t(s, x)). \quad (47)$$

Performing the integral we find  $M_0^0 \simeq \frac{\sqrt{3}}{2} a_0^0$  in the limit  $m_h \simeq 0$  (that is, much smaller than  $s$  and  $m_\rho$ ). The proportionality factor is easy to understand at least for small  $s$ . Just note that to project the elastic  $A$  over zero isospin we used  $A_0 = 3A(s) + A(t) + A(u)$  and that, since  $3s + t + u \simeq 2s$ ,  $A_0 = 2M$  for small  $s$ . Finally the  $\sqrt{3}$  comes from  $\sqrt{3}^{-1} \sum_a \delta^{aa}$  and reflects the different final state in  $A(\pi^a \pi^b)$  and  $M(hh)$ .

Comparing now with the nonlinear version of the Higgs effective field theory (EFT), where

$$M_0^0 = \frac{\sqrt{3}}{32\pi v^2} (a^2 - b)s + O(s^2), \quad (48)$$

it follows that

$$\left(K_1 + \frac{3K_2}{m_\rho^2}\right) = \frac{a^2 - b}{16\pi v^2} \quad (49)$$

and, by using Eq. (42), that

$$\frac{1}{16\pi f^2} = \frac{a^2 - b}{16\pi v^2}. \quad (50)$$

It further follows that  $a$  and  $b$  (independent parameters of the EFT) are correlated in CHMs by

$$(a^2 - b) = (1 - a^2) \quad (51)$$

that relates the strength of elastic scattering beyond the SM (rhs) with the inelastic one (lhs).

At higher order  $\mathcal{O}(s^2)$  in the expansion, strong vector resonances appearing in  $W_L W_L$  scattering leave sizable  $a_4$  and  $a_5$  coefficients. We do not pursue the topic further here but refer to [33] where the low-energy parameter map is studied in detail with attention to the appearance or not of a BSM vector resonance.

## B. Numerical results

We now numerically examine the elastic  $\pi^i \pi^j \rightarrow \pi^k \pi^l$  amplitudes as a function of the three independent parameters  $f$ ,  $m_\rho$  and  $\Gamma_\rho$  of scenario 1 ( $\hat{a}_\mu$ -decoupled).

In Fig. 2 we show the  $a_0^0$  scalar-isoscalar scattering amplitude as a function of Mandelstam- $s$ . We choose as reference parameter set  $m_\rho = 2$  TeV,  $f = 350$  GeV and  $\Gamma_\rho = 20\%m_\rho$  (thick, solid line). To show the dependence on parameters, the thick dashed and dotted lines correspond to increasing  $m_\rho$  to 4 and 6 TeV respectively. The red thin

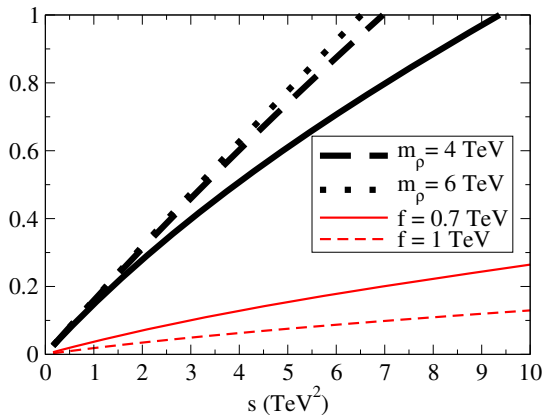


FIG. 2 (color online). Modulus of the scalar-isoscalar partial wave  $a_0^0$  (a real, positive number for real  $m_\rho$  and  $s$ ) in Eq. (34) as a function of Mandelstam- $s$ . Solid line: reference values of the parameters,  $m_\rho = 2$  TeV,  $f = 350$  GeV, with the thickness of the line representing the uncertainty in the width  $\Gamma_\rho \in (5 - 20\%)$ . Thick dashed and dotted lines: same with  $m_\rho = 4$  and 6 TeV. Red thin lines: instead, increase  $f$  to 0.7 and 1 TeV (at the larger  $\Gamma_\rho = 0.2m_\rho$  width value and  $m_\rho = 2$  TeV).

ones towards the bottom of the plot correspond to  $m_\rho = 2$  TeV and increasing  $f$  to 0.7 and 1 TeV instead. The width of the vector state exchanged in the  $t, u$  channels is of little concern for this scalar-channel amplitude. The thickness of the line itself corresponds to varying the width between 5% and 20%. The unitarity bound  $\text{Re}(a_0^0) \leq \frac{1}{2}$  is violated at around 1.7 TeV, invalidating perturbation theory. This happens at lower energies for larger  $m_\rho$  and at higher energies for larger  $f$ : for the higher  $f$  values shown, the violation of unitarity happens at higher scales between 4 and 5 TeV.

One effect in the perturbative amplitude of adding the width of the vector resonance (induced by its potentially large coupling to fermions, for example) is the appearance of an imaginary part in the  $a_0^0$  amplitude because of the substitution  $m_\rho \rightarrow (m_\rho - i\frac{\Gamma_\rho}{2})$  in Eq. (34). In Fig. 3 we separately plot the real and imaginary parts of  $a_0^0$ . Though now complex,  $a_0^0$  still fails the unitarity test that would only be satisfied perturbatively if an NLO amplitude was added: the induced imaginary part is too small.

Since adding or not a width  $\Gamma_\rho$  will not change any of our qualitative statements, particularly in Fig. 11 below, we will subsequently fix  $\Gamma_\rho$  in Eq. (34) to the larger value  $\Gamma_\rho/m_\rho = 20\%$  when dealing with the scalar channel in this subsection, and neglect  $\Gamma_\rho$  altogether afterwards (in the vector channel it does make a difference as we explain next).

The isotensor wave  $a_2^0$  is repulsive and thus not expected to resonate at low energy, and since its value is  $-a_0^0/2$  we do not plot it explicitly.

The vector-isovector wave is shown in turn, again in perturbation theory, in Fig. 4. Unitarity is here perfectly respected in all the low and intermediate energy region up to a few TeV, and it is saturated of course at  $m_\rho = 2$  TeV, where  $|a_1^1| = 1$  for the narrower resonance. Other values of  $m_\rho$  trivially displace the pole; but it is worth showing how this channel reacts to  $\Gamma_\rho$ , to which we assign the two values

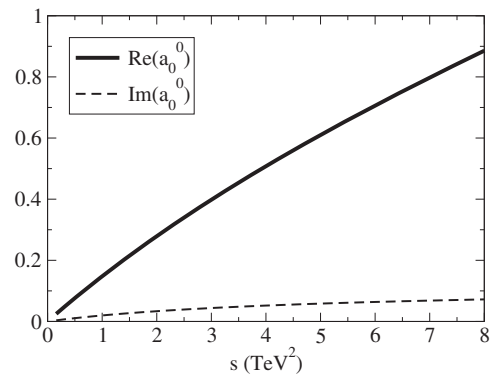


FIG. 3. We plot the scalar-isoscalar partial wave in Eq. (34) explicitly showing the real and imaginary parts. The later comes from the substitution  $m_\rho \rightarrow (m_\rho - i\frac{\Gamma_\rho}{2})$  with  $m_\rho = 2$  TeV,  $\Gamma_\rho = 20\%m_\rho$ ,  $f = 350$  GeV.

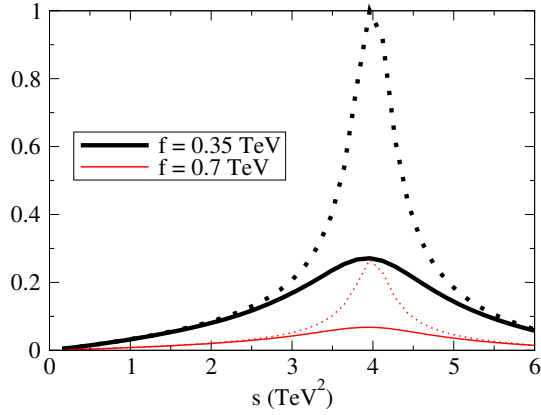


FIG. 4 (color online). Modulus of the vector-isovector partial wave  $|a_1^+|$  in Eq. (35) as a function of Mandelstam- $s$ . Solid lines:  $\Gamma_\rho = 20\%m_\rho$ . Dotted lines:  $\Gamma_\rho = 5\%m_\rho$  for  $m_\rho = 2$  TeV.

5% and 20%. We also display the calculation for two values of  $f$ . It is seen that the peak is more prominent for small  $f$ , while larger values of  $f$  tend to make it disappear (this is because of the smaller  $K_2$ , coupling intensity of the resonance to the  $\pi\pi$  channel, at fixed  $m_\rho$ ).

Figure 5 displays in turn the tensor-isoscalar amplitude  $a_2^0$ . This partial wave is seen to be very small (note the scale in the y-axis has been divided by 10), far from reaching the unitarity bound  $\text{Re}(a_2^0) \leq \frac{1}{2}$ , and thus perturbative and nonresonating. In comparing with the  $J=0$  wave in Fig. 2, we see that the convergence of the partial wave expansion of the amplitude in the low-energy region is excellent, with the isoscalar channel practically dominated by the lowest, scalar partial wave. This is analogous to the QCD situation where the scalar  $\sigma$  pole at 450 MeV dominates low-energy  $\pi\pi$  scattering, with the first tensor resonance, the  $f_2(1270)$ , being much higher in mass. A difference between the scalar and tensor channels is their reaction to increasing  $m_\rho$ . While in the scalar channel this makes the amplitude larger bringing unitarity violation to a

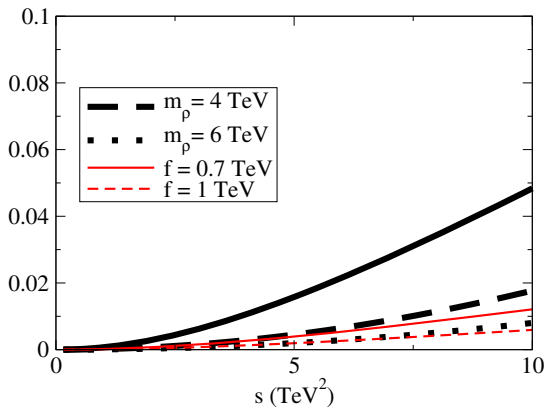


FIG. 5 (color online). Tensor-isoscalar partial wave  $a_2^0$ . Lines as in Fig. 2.

smaller scale, in the tensor channel it makes it smaller just like increasing  $f$  does.

We now turn to the second scenario from Table I. We shade the plots with numerical data from this scenario 2 (soft yellow online) to easily distinguish them. In Fig. 6 we compare both scenarios. We have fixed  $f$ ,  $m_\rho$  and  $\Gamma_\rho$  and vary only  $g_s$  in scenario 2, which is a free parameter controlling the coupling of the vector to the  $\pi\pi$  channel (the remaining width presumably due to fermion couplings). As can be seen, the results at low energy are not too disparate, and the second scenario converges towards the first when  $m_{\tilde{a}} \rightarrow \infty$  (the largest such mass in the plot is about 16 TeV and corresponds to the  $g_s = 4$  curve).

In Figs. 6 and 7 we stay with scenario 2, assuming the 4DCHM without decoupling the axial vector resonances. The first of them offers a comparison with scenario 1 in the limit  $m_{\tilde{a}} \rightarrow \infty$ , achieved for a finite value of  $g_s$  for which  $f_2 \rightarrow \infty$ . As seen in the plot, the convergence is good though not monotonic in sign. In any case, the two scenarios seem to give comparable results for both values of  $f = 0.35$  and  $0.7$  TeV.

Further detail is provided by Fig. 7. Here  $f = 350$  GeV, so the imaginary part of the scalar channel in the top plot is directly comparable with the real part in the top plot in Fig. 6. In the real part, unitarity is clearly violated by

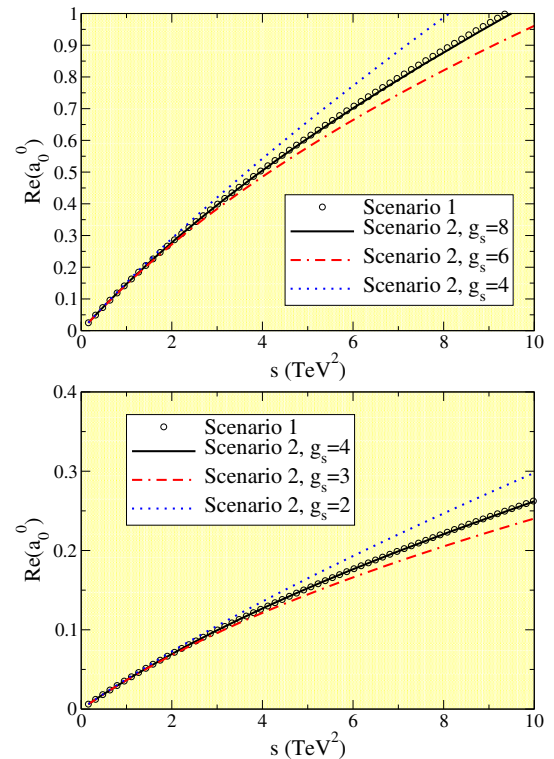


FIG. 6 (color online). Scenario 2 converges towards scenario 1 for a certain  $g_s$ . With the parameters here ( $m_\rho = 2$  TeV,  $\Gamma_\rho = 20\%m_\rho$ ), this happens for  $g_s$  slightly larger than 8 if  $f = 0.35$  TeV (top plot) and for  $g_s$  a bit above 4 for  $f = 0.7$  TeV (bottom).

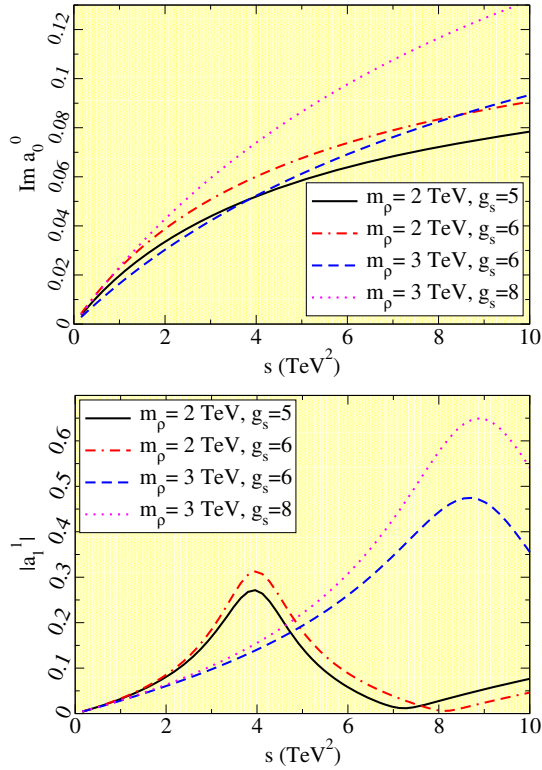


FIG. 7 (color online). Scenario 2, the complete 4DCHM. Top: imaginary part of the scalar, isoscalar partial wave. Bottom: modulus of the vector, isovector one. Here,  $f = 350$  GeV and  $\Gamma_\rho/m_\rho = 20\%$ .

exceeding the bound  $\text{Re}(a_0^0) \leq \frac{1}{2}$ . The imaginary part shows additionally that the relation  $\text{Im}(a_0^0) = |a_0^0|^2$  is not satisfied even when the bound is not exceeded (the imaginary part is of order 0.01–0.02 in the low-energy region).

For the shown values of  $g_s$ ,  $m_{\hat{a}}$  is either half a TeV or a TeV higher than  $m_\rho$ , so its effect in the low-energy physics is less prominent, but it is not totally decoupled as in scenario 1 (we have not included the  $\hat{a}$  exchanges in our computation because, as stated in Sec. II, the  $\hat{a}$  have small couplings to  $\pi\pi$  induced by EWSB and their contribution to the unitarity dynamics is negligible).

The lower plot in Fig. 7 shows the vector-isovector wave that behaves unsurprisingly, peaked at the nominal mass, with the width that we have fixed *a priori*, and with a strength that grows with  $g_s$ , its coupling to the  $\pi\pi$  channel (when  $\Gamma_{\pi\pi} \rightarrow \Gamma_\rho$  the peak height of the modulus approaches 1, saturating unitarity).

## V. COUPLED CHANNEL UNITARITY

### A. Analysis for physical $s$

An unpleasant feature of perturbation theory is the breakdown of unitarity that can be catastrophic if the interactions become relatively strong, even surpassing the unitarity bound. This limits the reach of effective

low-energy Lagrangians, but dispersion-relation based analysis provides a way around. There are several tools and methods of varying sophistication to address unitarity, but for this exploration we adopt the simplest, so-called “K-matrix” method [34] (see [35] and [36] for a related work and a recent extension of this prescription). In its original form, this guarantees unitarity but not the appearance of a proper right cut, so we use a slightly modified version, sometimes called “improved K-matrix” approach. It is based on the observation that the often appearing loop function

$$J(s) = \frac{-1}{\pi} \log\left(\frac{-s}{\Lambda^2}\right) \quad (52)$$

provides a right-hand cut in the complex- $s$  plane for  $s \in (0, \infty)$ . Here  $\Lambda$  is an appropriate high-energy cutoff that we can naturally take as  $\Lambda = m_\rho$  to analyze the lower-energy scalar channel.

If the amplitude  $M(\pi^i\pi^j \rightarrow \pi^4\pi^4)$  vanished, we could unitarize the elastic  $A(\pi^i\pi^j \rightarrow \pi^i\pi^j)$  scalar amplitude as  $\tilde{a} = a(1 - Ja)^{-1}$ . This amplitude would satisfy  $\text{Im} a = |a|^2$ , but mixing with the Higgs-Higgs channel introduces the inelastic scalar  $m_0^0$  projection of Eq. (47) in this relation. This happens only in the isospin-zero channel where there is mixing between the  $W_L W_L$  and Higgs-Higgs states because of the nonvanishing channel-coupling amplitude in Eq. (29). Thus, we expect a probability leak from the  $\pi^i\pi^j$  to the  $\pi^4\pi^4$  channels.

Under this circumstance, the exact elastic unitarity relation that the amplitude needs to satisfy is

$$\text{Im} a = |a|^2 + |m|^2 \quad (53)$$

(the 0 indices are omitted). A convenient way to implement it is to construct a reaction matrix that contains both channels in perturbation theory,

$$k = \begin{pmatrix} a & m \\ m & 0 \end{pmatrix} \quad (54)$$

(noticing the vanishing of the Higgs-Higgs elastic amplitude in LO perturbation theory, a model feature). This perturbative  $2 \times 2$  reaction matrix can be unitarized by

$$\tilde{k} = k(1 - Jk)^{-1} \quad (55)$$

if  $k$  is small, which happens at low  $s$ , so this model amplitude reproduces the LO perturbative behavior since  $\tilde{k} \simeq k + \dots$  therein.

The unitarization prescription of the K-matrix is by no means unique, with alternatives being the large- $N$  treatment, the inverse amplitude method (IAM), or the  $N/D$  ansatz [37], but all yield qualitatively similar results in the

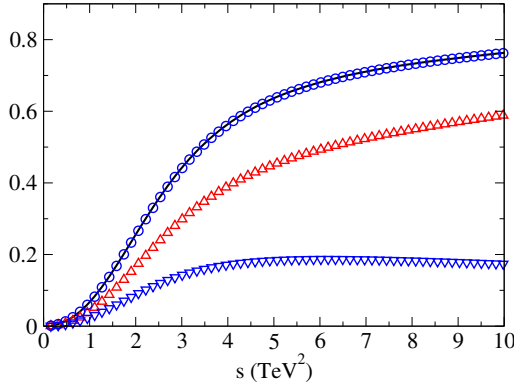


FIG. 8 (color online). Test of unitarity for  $\text{Im } \tilde{a} = \text{Im } \tilde{k}_{11}$  (black solid line). Bottom line (downward triangles, blue online):  $|\tilde{m}|^2 = |\tilde{k}_{12}|^2$ . Second from bottom (upward triangles, red on-line):  $|\tilde{a}|^2 = |\tilde{k}_{11}|^2$ . Circles (on top of the imaginary part): the sum of the last two, unitarity compliant. Here  $\Gamma_\rho/m_\rho = 5\%$ , for larger values a small difference is visible due to the perturbative  $a_0^0$  acquiring an imaginary part.

scalar channel over the right cut (the physical  $s$  region) and nearby in the complex plane.

The matrix element  $\tilde{k}_{11} \equiv \tilde{a}$  thus substitutes  $a_0^0(s)$  for all but the lowest energies. Its explicit expression is

$$\tilde{a} = \frac{a + Jm^2}{1 - Ja - J^2m^2}. \quad (56)$$

Equation (53) is now satisfied exactly as long as the perturbative  $a$  is real. Since  $\Gamma_\rho$  was shown to induce a small imaginary part in the perturbative scalar amplitude, there is a residual unitarity problem of that same order. To avoid it, and since the effect of the width was numerically small in the scalar channel, we neglect  $\Gamma_\rho$  here altogether.

In Fig. 8 we present one of the three possible checks of unitarity for the  $K$  matrix (in scenario 1 for definiteness), showing the satisfaction of Eq. (53) for the  $\tilde{a} = \tilde{k}_{11}$  and  $\tilde{m} = \tilde{k}_{12}$  quantities (the other two independent checks are also satisfied, but not shown).

By comparing the lowest two curves in the figure one can see that after unitarization the loss of probability from the  $W_L W_L$  channel to the  $hh$  channel is still about 25% of the elastic scattering one.

In Fig. 9 we then present the modulus of the elastic amplitude (after unitarization)  $|\tilde{k}_{11}| = |\tilde{a}_0^0(s)|$  that shows how the goal has been met: the amplitude equals the LO perturbation theory for the lowest  $s$  but later moderates its growth satisfying the theoretical constraints. In both scenarios it is apparent that the presence of a  $\rho$ -boson at low energy and strongly coupled to the  $\pi\pi$  channel weakens the strength of the scalar channel and makes it more perturbative.

Other unitarization methods will lead to qualitatively similar predictions. To make an appreciable gain in

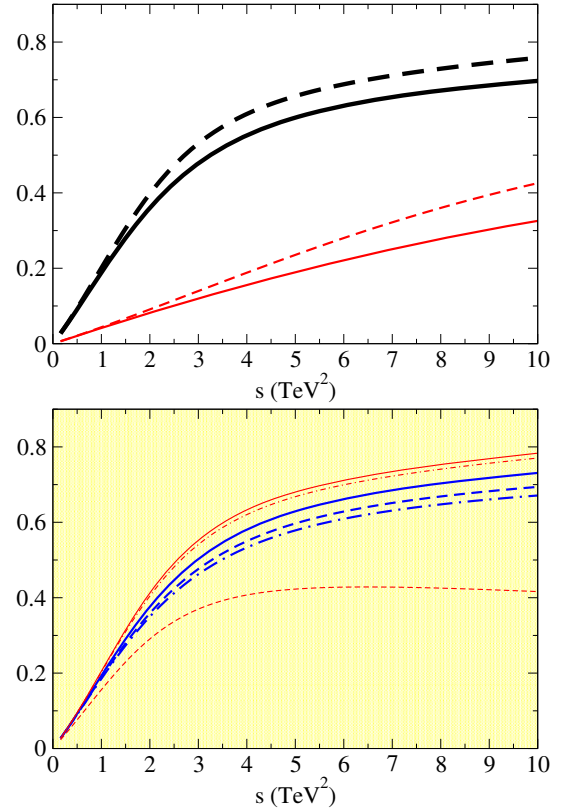


FIG. 9 (color online). Modulus of the unitarized elastic matrix element  $|\tilde{k}_{11}| = |\tilde{a}_0^0(s)|$ , that remains below 1 in all the energy interval of interest. First plot (scenario 1): solid lines correspond to  $m_\rho = 2$  TeV, dashed ones to  $m_\rho = 4$  TeV. From thicker to thinner,  $f = 0.35, 0.7$  TeV respectively. Lower plot: in scenario 2, we fix  $f = 0.35$  TeV and  $\Gamma_\rho/m_\rho = 5\%$ . The thick lines (blue online) correspond to  $m_\rho = 2$  TeV, with  $g_s = 4$  (solid), 6 (dash-dotted) and 8 (dashed). The thin ones (red online) were in turn calculated with  $g_s = 6$  (solid), 8 (dash-dotted) and 10 (dashed), and all have  $m_\rho = 4$  TeV.

accuracy, if ever necessary, the complete NLO amplitudes would have to be calculated and then fed into the more sophisticated IAM [38] (that requires both LO and NLO).

An interesting feature that illustrates the limitations of perturbation theory is presented in Fig. 10 that shows the modulus  $|\tilde{k}_{22}| = |\tilde{t}_0^0(s)|$  of the elastic  $hh \rightarrow hh$  or  $\pi^4 \pi^4 \rightarrow \pi^4 \pi^4$  scattering amplitude for zero angular momentum. It is remarkable that the scattering amplitude takes a finite and indeed non-negligible value when it is zero in LO perturbation theory. This reflects in the figure in that the linear term near the origin is zero, but the amplitude quickly overcomes this and takes appreciable values. This effect occurs, of course, by rescattering through the other channel,  $hh \rightarrow W_L W_L \rightarrow hh$ , and since the unitarization procedure typically resums the imaginary part of all such rescatterings, it is able to yield a finite value even when only LO perturbation theory is at hand.

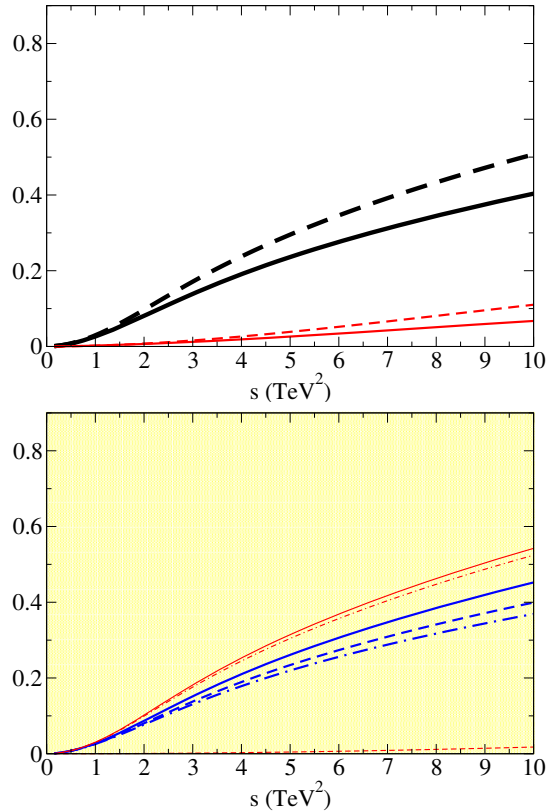


FIG. 10 (color online). Same as Fig. 9 but for  $|\tilde{k}_{22}| = |\tilde{z}_0^0(s)|$  the elastic  $hh \rightarrow hh$  scattering that vanishes in the perturbative amplitude at LO. Unitarization requires this channel to have finite probability too.

### B. Extension to the complex $s$ -plane: $\sigma$ pole

The most important midrange attraction of the nucleon-nucleon potential in nuclear physics is controlled by an exchange with scalar quantum numbers, that is usually assigned to a  $\sigma$  particle. In the modern understanding of QCD, this particle, perhaps too broad to be called as such, is a resonance or pole in the second Riemann sheet of the scattering amplitude  $\pi\pi \rightarrow \pi\pi$  with a mass of about 450 MeV. It is now known with remarkable precision thanks to the use of accurate dispersion relations with a wealth of low and midenergy data. The strong interaction that we observe in  $W_L W_L$  scattering in Fig. 9 also comes from an equivalent pole in the second Riemann sheet. To expose it with the  $K$ -matrix method (obviously a model, thus less precise than the Roy equations [39,40] that can later be applied when/if data becomes available) we extend the variable  $s$  to the complex plane in our computer code. The extension to the second Riemann sheet, where resonance poles in the lower-half plane can appear (since they are forbidden in the first sheet due to causality) is implemented in the loop function in Eq. (52). It is sufficient to take the logarithm to be cut in  $(-\infty, 0)$  (so the argument is defined between  $-\pi$  and  $\pi$ ) and exploit the simple prescription

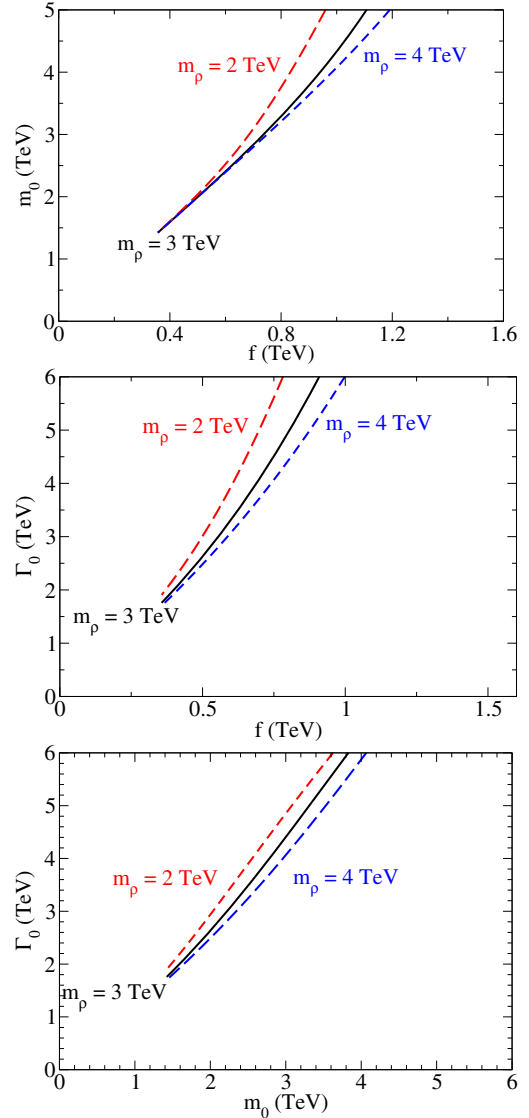


FIG. 11 (color online). Top and middle plots: evolution of the mass and width of the dynamically generated scalar  $\sigma$ -like resonance as function of  $f$  in the limit  $f_2 \rightarrow \infty$  (scenario 1), for three values of the vector mass. Bottom: width of the scalar resonance against its mass, with  $f$  being now just the parameter of the trajectory in this plane.

$$\log \left( \frac{-s}{m_\rho^2} \right)_{\text{II}} = \log \left( \text{Abs} \left( \frac{s}{m_\rho^2} \right) \right) + i \left( \text{Arg} \left( \frac{s}{m_\rho^2} \right) - \pi \right). \quad (57)$$

We then employ the CERN standard minimization program MINUIT to search the complex plane for zeros of the determinant of  $(1 - Jk)$  that yield the poles of the unitarized scattering amplitude  $\tilde{k}$ , in accord with Eq. (55). We find exactly one such pole and interpret its position as an effective resonance with a certain mass and width, given by  $\sqrt{s} = M_0 - i\Gamma_0/2$  (where the 0 reminds us of its apparent spin).

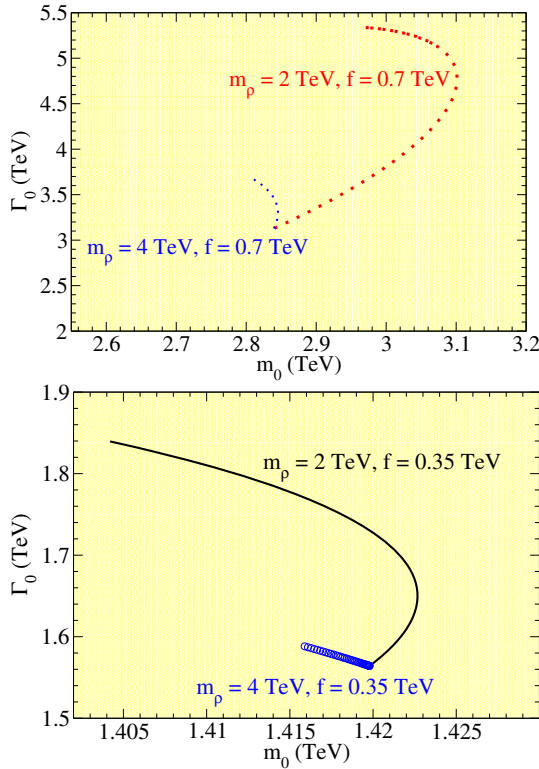


FIG. 12 (color online). Varying  $g_s$  produces a curve in the  $(m_0, \Gamma_0)$  plane of the  $\sigma$ -like pole as extracted from its complex- $s$  position, for  $f = 0.7$  TeV (top) and  $f = 0.35$  TeV (bottom), and for  $m_\rho = 2$  or 4 TeV as indicated. It may happen that for each value of  $m_0$  there are two values of  $\Gamma_0$ . This reflects the oscillation with the parameter of the curve,  $g_s$ , visible in Fig. 13, and caused by the nontrivial dependence of Eq. (31) on  $g_s$ .

We have tracked the evolution of this pole in scenario 1 for fixed  $\Gamma_\rho/m_\rho = 0.05$  as a function of  $f$  and for three values of  $m_\rho$  as shown in Fig. 11. We show the behavior of the mass and width of the scalar pole in terms of  $f$  in the first two plots, then eliminate this parameter to see directly  $\Gamma_0(m_0)$  in the third plot.

As the LHC data advances and perhaps tightens the constraint on  $f$  rising its minimal allowed value, the possible positions of the pole recede in the complex plane (larger  $m_0$  and  $\Gamma_0$  for larger  $f$ , at fixed  $m_\rho$ ).

If, in contrast, the vector resonance relatively decouples from the low energy Goldstone bosons, because of its heavy mass (large  $m_\rho$ ), we recover the known broad pole from generic strongly interacting theories a bit under 2 TeV. As the  $\rho$  becomes lighter, this pole moves up in energy (for fixed  $f$ ) and becomes broader. Since its width is similar in size to its mass (bottom plot) for all values of  $f$  (bottom plot of Fig. 11) its interpretation as an unstable particle is as difficult as in QCD.

We now turn to scenario 2 (the full 4DCHM with a finite  $m_a$  mass, though we still neglect its exchange) and plot the result in Figs. 12 and 13.

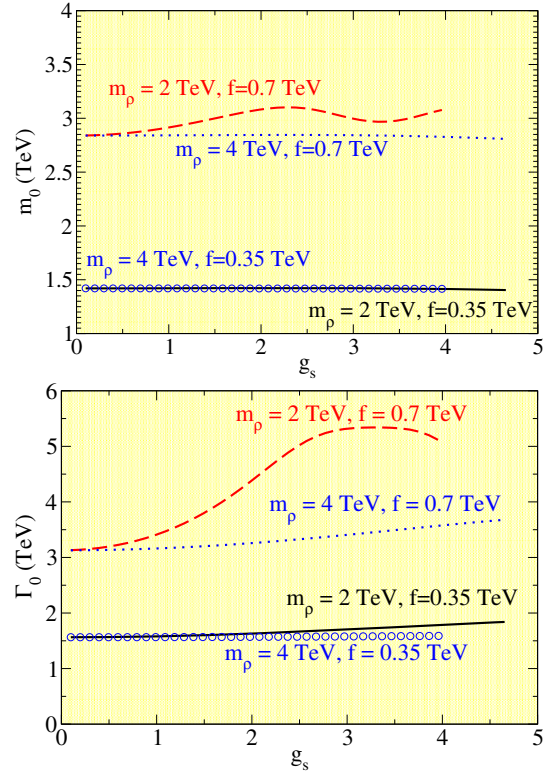


FIG. 13 (color online). Evolution of the mass (top) and width (bottom) of the dynamically generated scalar  $\sigma$ -like resonance as a function of  $g_s$  in scenario 2, for fixed vector masses 2 and 4 TeV and fixed  $f = 0.35$  and 0.7 TeV as indicated.

The top plot of Fig. 12 shows the complex-plane evolution (with  $g_s$  being the curve's parameter) for fixed  $f = 0.35$  TeV and  $m_\rho = 2$  or 4 TeV, while the bottom one corresponds to the same  $m_\rho$  but a larger  $f = 0.7$  TeV. In comparing with the bottom plot of Fig. 11 we see that the dependence of the mass and width on  $f$  and  $m_\rho$  is similar: larger  $f$  entails a heavier and broader pole, while a heavier  $m_\rho$  moves it the opposite way, towards lighter values of  $m_0$  and  $\Gamma_0$ . The pole position bends gently in the complex plane, which must translate into a slight oscillation as a function of  $g_s$ . This is observed in Fig. 13 where we represent  $m_0$  and  $\Gamma_0$  as a function of  $g_s$ .

The most noticeable effect is that the mass is practically independent of  $g_s$  except for larger  $f$  and smaller  $m_\rho$ , where it fluctuates somewhat more. The curves in both figures end when  $g_s$  is so large that either  $f_2$  is very large or  $\Gamma_{\rho\pi\pi}$  equals its maximum possible value  $\Gamma_\rho$  that we have set in both cases to 5% of  $m_\rho$ .

The width of the scalar pole moves slightly up with that of the vector pole, but in all the effect of  $g_s$  is not striking (for moderate widths of the vector resonance itself  $\Gamma_\rho$ ).

So the conclusion from both scenarios is how the  $\sigma$  pole recedes deeper in the complex plane as  $f$  is increased, and its mass behaves opposite to the vector one for fixed couplings.

Thus, if the vector resonance is coupled as the symmetries of the CHM dictate, it not only unitarizes the vector channel with its quantum numbers, but it also improves perturbative unitarity in the scalar channel (not generically true for other low-energy vector resonances).

## VI. $\rho\rho$ PRODUCTION

We now make a slight extension of our low-energy study and take a look at the  $\rho\rho$  threshold. Double- $\rho$  intermediate states should be taken into account in the elastic  $\pi\pi$  amplitude, but we will not recalculate those and leave it to future investigation. Nevertheless, for completeness, we find interesting to explore the inelastic scattering amplitude  $B(\pi^a\pi^b \rightarrow \rho_L^c\rho_L^d)$ , containing  $h$ ,  $\pi$  and  $\rho$  exchange channels, and with a general isospin structure:

$$B^{ab\rightarrow cd} = A(s, t, u)\delta^{ab}\delta^{cd} + B(s, t, u)\delta^{ac}\delta^{bd} + B(s, u, t)\delta^{ad}\delta^{bc}. \quad (58)$$

We quote explicit expressions for  $A(s, t, u)$  and  $B(s, t, u)$ , where threshold effects will be important (if the threshold

$$A(s, t, u) = \frac{g_s^2}{4} \left( \frac{f^2}{2f_1^2} + \frac{f^2}{f_2^2} \right)^2 \frac{1}{m_\rho^2\beta_\rho^2} \frac{1}{u} \left( \frac{s}{2}(\beta_\rho^2 + 1) + t - m_\rho^2 \right)^2 + \frac{g_s^2}{4} \left( \frac{f^2}{2f_1^2} + \frac{f^2}{f_2^2} \right)^2 \frac{1}{m_\rho^2\beta_\rho^2} \frac{1}{t} \left( \frac{s}{2}(\beta_\rho^2 - 1) - t + m_\rho^2 \right)^2, \quad (59)$$

$$B(s, t, u) = \frac{g_s^2}{4} \left( \frac{f^2}{2f_1^2} + \frac{f^2}{f_2^2} \right) \left[ \frac{(s + 2m_\rho^2)(t - u)}{(s - m_\rho^2)m_\rho^2} + \left( \frac{f^2}{2f_1^2} + \frac{f^2}{f_2^2} \right) \frac{1}{m_\rho^2\beta_\rho^2} \times \left( \frac{(\frac{s}{2}(\beta_\rho^2 + 1) + t - m_\rho^2)^2}{u} + \frac{(\frac{s}{2}(\beta_\rho^2 - 1) - t + m_\rho^2)^2}{(t - m_\rho^2)} \right) \right]. \quad (60)$$

As we have  $m_h \ll m_\rho$ , it is justified to take the massless  $m_h \rightarrow 0$  limit in this amplitude. Since the LHC might reach the  $\rho\rho$  threshold but would probably be energy and luminosity constrained to go much above, in practice, we need consider only the scalar partial wave (higher ones being suppressed by powers of  $p^l$ ). After projecting, and setting  $m_h = 0$ , we get

$$b_0^0(s) = K_2 \frac{5}{8\beta_\rho^2 m_\rho^2} \left[ (1 - 2\beta_\rho^2)s - 2m_\rho^2 + \frac{((1 - \beta_\rho^2)s - 2m_\rho^2)^2}{2\beta_\rho s} \log \left( \frac{(1 - \beta_\rho)s - 2m_\rho^2}{(1 + \beta_\rho)s - 2m_\rho^2} \right) \right] \quad (61)$$

for the  $\rho\rho$  production inelastic amplitude with entrance channel  $\pi\pi$ . This amplitude is real and negative for  $s > 4m_\rho^2$  (note the logarithm itself is negative).

The scalar-isoscalar projection in Eq. (61) is shown in Fig. 14 with the threshold at  $E_0 = 2m_\rho = 4$  TeV ( $s_0 = 16$  TeV<sup>2</sup>). We are allowed to vary the value of  $g_s$  and  $f$ , but need to ensure  $f_2^2 > 0$ . The amplitude is finite at the double- $\rho$  threshold. Notice from Fig. 14 that the modulus of the amplitude grows most linearly in the perturbation theory, and we are able to have the linear term finely tuned to avoid stringent constraint from the inelastic scattering channel. However it will ultimately violate unitarity in the large  $s$  limit. We abstain from

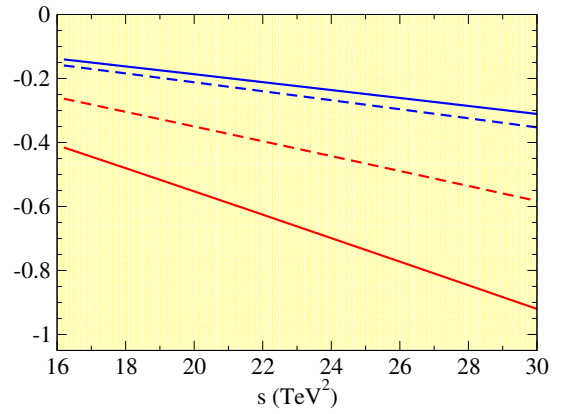


FIG. 14 (color online). Scalar-isoscalar perturbative amplitude of  $\pi\pi \rightarrow \rho_L\rho_L$  for  $m_\rho = 2$  TeV, with  $g_s = 3$  (dashed line) and  $g_s = 4$  (solid line) in scenario 2. The two bottom lines and the two top lines correspond respectively to  $f = 0.35$  and 0.7 TeV.

can be reached at all), and are encoded in the phase-space velocity factor  $\beta_\rho = \sqrt{1 - 4m_\rho^2/s}$  [41].

unitarizing it at the current stage since, at such a energy scale, one should start thinking whether other resonances should be included into the effective theory.

## VII. CONCLUSIONS

In this paper we have examined a simple CHM template with vector resonances assumed to be accessible at the LHC. As CHMs naturally come with a family of such new states, both charged and neutral, we have implicitly taken the pragmatic approach (in the sense that it enabled us to perform accurate numerical studies that would otherwise not be possible) of assuming that the CERN collider will

find initially only one (degenerate) pair of such states. This could be the lowest lying one in terms of mass or else the most strongly interactive one with SM matter.

After obtaining the scattering amplitudes among the low-energy particles,  $W_L$  and  $h$ , their partial wave projections, and adopting the improved  $K$ -matrix method of unitarization, we have exposed an effective scalar resonance (equivalent to the  $\sigma$  meson of low-energy hadron physics), wherein the keyword “effective” is meant to highlight the fact that this object, other than being a proper spin-0 state, could well appear as such yet being the scalar polarization of one or more of the additional vector resonances naturally present in CHMs but not seen at the LHC, even lighter than the detected  $\rho$  states (if weakly coupled to SM objects). In fact, the proliferation of new gauge resonances typical of CHMs can also account for the rather broad appearance of the new  $\sigma$  state. For example, its pole may well be just the typical mass scale of the unseen spin-1 states and its width the linear sum of the individual ones. This is well known to be realizable in case of multiple, nearly overlapping and typically narrower Breit-Wigner shapes with or without additional phases related to pole residues [42]). In our case, such states would be taken from the coset (or even from additional sites). The decay dynamics also leaves plenty of scope in a typical CHM for adequate interpretation. It should indeed be recalled that the aforementioned vector resonances come accompanied in these scenarios by a variety of heavy fermions, the former decaying into the latter, with the fermionic masses and couplings dictating the size of the width of both the  $\rho$  states and other vector bosons present in the spectrum. This was emphasized and quantitatively illustrated in [15] in one specific CHM realization, the so-called 4DCHM, which we have used as a reference benchmark herein. However, in this connection, a caveat should be borne in mind. Since in the 4DCHM there is no space for vector resonances lighter than  $\rho_{L,R}$ <sup>3</sup> which are also the most strongly coupled ones to SM matter and forces, we can interpret our results by saying that, if we want this construct to satisfy perturbative

<sup>3</sup>An exception is the gauge boson associated with an extra U(1) symmetry, necessary for the correct hypercharge assignment to the SM fermions, which however is weakly coupled to  $W_L W_L$ .

unitarity, we must require  $f$  to be larger than the threshold value for which  $m_0 > m_\rho$ . Also, we need to invoke spin-1 resonances with larger mass and width, not included in the 4DCHM, which is a two-sites truncated theory describing only the lowest lying resonances, to realize the “sigma” as a cooperative effect.

Whichever the underlying CHM realization though, the position in the complex  $s$ -plane of this resonance should depend slightly on the partial width of the  $\rho$ s but more strongly on the vector mass  $m_\rho$  with an inverse relation, so when one becomes lighter, the other is heavier and vice versa.

Altogether, when all the relations among parameters in the CHMs at hand are taken into account, the presence of the  $\rho$  at fixed  $f$  improves perturbative unitarity and pushes the effective scalar pole deeper into the complex plane. It will therefore be crucial, in the case of a  $\rho$  state discovery at the LHC, to closely scrutinize its properties in order to ascertain, through the unitarization method that we have advocated here, whether and where additional states above and beyond the SM spectrum can be found. We therefore conclude that, unless specific model assumptions are made on the nature of a  $\rho$  state accessible at the LHC, the unitarization procedure adopted here is a powerful method to gain substantive knowledge (mass, width, spin, etc.) of the yet unseen spectrum of the CHM at hand, either lighter or heavier than the  $\rho$  itself, in a model-independent approach. In fact, such an approach can be extended to incorporate further discoveries of both vector and scalar states that might occur at the LHC in the years to come.

## ACKNOWLEDGMENTS

F. J. L. E. thanks instructive conversations with A. Dobado, particularly about Eq. (57), and support from Grants No. MINECO: FPA2014-53375-C2-1-P and No. MINECO:FPA2011-27853-01 as well as computer resources, technical expertise and assistance from the Red Española de Supercomputación. F. J. L. E. also thanks the Southampton High Energy Physics (SHEP) group for hospitality at the time when this project was conceived. S. M. is financed in part through the NExT Institute. S. M. also acknowledges insightful discussions with R. L. Delgado. H. Cai is supported in part by the postdoc foundation under Grant No. 2012M510001.

[1] G. Aad *et al.* (ATLAS Collaboration), Observation of a new particle in the search for the Standard Model Higgs boson with the ATLAS detector at the LHC, *Phys. Lett. B* **716**, 1 (2012); S. Chatrchyan *et al.* (CMS Collaboration), Observation of a new boson at a mass of 125 GeV with the CMS experiment at

the LHC, *Phys. Lett. B*, **716**, 30 (2012); G. Aad *et al.* (ATLAS Collaboration), Observation and study of the Higgs boson candidate in the two photon decay channel with the ATLAS detector at the LHC, Report No. ATLAS-CONF-2012-168; S. Chatrchyan *et al.* (CMS Collaboration), Evidence for a new

- state decaying into two photons in the search for the standard model Higgs boson in pp collisions, Report No. CMS-HIG-12-015.
- [2] Precise exclusion limits within specific models have been recently reported in V. Khachatryan *et al.* (CMS Collaboration), Search for massive resonances decaying into pairs of boosted bosons in semi-leptonic final states at  $\sqrt{s} = 8$  TeV, *J. High Energy Phys.* **08** (2014) 174; V. Khachatryan *et al.* (CMS Collaboration), Search for new resonances decaying via WZ to leptons in proton-proton collisions at  $\sqrt{s} = 8$  TeV, [arXiv:1407.3476](https://arxiv.org/abs/1407.3476).
- [3] D. B. Kaplan and H. Georgi, SU(2) $\times$ U(1) breaking by vacuum misalignment, *Phys. Lett.* **136B** 183 (1984).
- [4] K. Agashe, R. Contino, and A. Pomarol, The minimal composite Higgs model, *Nucl. Phys.* **B719**, 165 (2005).
- [5] J. M. Cornwall, D. N. Levin, and G. Tiktopoulos, Derivation of gauge invariance from high-energy unitarity bounds on the s matrix, *Phys. Rev. D* **10**, 1145 (1974); C. E. Vayonakis, Born helicity amplitudes and cross-sections in nonabelian gauge theories, *Lett. Nuovo Cimento* **17**, 383 (1976); B. W. Lee, C. Quigg, and H. Thacker, Weak interactions at very high-energies: the role of the Higgs boson mass, *Phys. Rev. D* **16**, 1519 (1977); M. S. Chanowitz and M. K. Gaillard, The TeV physics of strongly interacting W's and Z's, *Nucl. Phys.* **B261**, 379 (1985); M. S. Chanowitz, M. Golden, and H. Georgi, Low-energy theorems for strongly interacting W's and Z's, *Phys. Rev. D* **36**, 1490 (1987); A. Dobado and J. R. Peláez, On the equivalence theorem in the chiral perturbation theory description of the symmetry breaking sector of the standard model, *Nucl. Phys.* **B425**, 110 (1994); On the equivalence theorem in the chiral perturbation theory description of the symmetry breaking sector of the standard model, *Phys. Lett. B* **329**, 469 (1994); The equivalence theorem for chiral lagrangians, *Phys. Lett. B* **335**, 554 (1994).
- [6] S. Kanemura, K. Kaneta, N. Machida, and T. Shindou, New resonance scale and fingerprint identification in minimal composite Higgs models, [arXiv:1410.8413](https://arxiv.org/abs/1410.8413).
- [7] F. Siringo, Light Higgs bosons from a strongly interacting Higgs sector, *Europhys. Lett.* **59**, 820 (2002).
- [8] R. L. Delgado, A. Dobado, and F. J. Llanes-Estrada, Light, yet strong interactions, *J. Phys. G* **41**, 025002 (2014).
- [9] G. Bhattacharyya, D. Das, and P. B. Pal, Modified Higgs couplings and unitarity violation, *Phys. Rev. D* **87**, 011702 (2013).
- [10] A. Lahiri and D. Mukhopadhyay, Unitarity in  $WW \rightarrow WW$  elastic scattering without a Higgs boson, [arXiv:1107.1501](https://arxiv.org/abs/1107.1501).
- [11] L. Basso, S. Moretti, and G. M. Pruna, Theoretical constraints on the couplings of nonexotic minimal Z' bosons, *J. High Energy Phys.* **08** (2011) 122.
- [12] R. Contino, D. Marzocca, D. Pappadopulo, and R. Rattazzi, On the effect of resonances in composite Higgs phenomenology, *J. High Energy Phys.* **10** (2011) 081.
- [13] K. Agashe, H. Davoudiasl, S. Gopalakrishna, T. Han, G. Y. Huang, G. Perez, Z. G. Si, and A. Soni, LHC signals for warped electroweak neutral gauge bosons, *Phys. Rev. D* **76**, 115015 (2007).
- [14] K. Agashe, S. Gopalakrishna, T. Han, G. Y. Huang, and A. Soni, LHC signals for warped electroweak charged gauge bosons, *Phys. Rev. D* **80**, 075007 (2009).
- [15] D. Barducci, A. Belyaev, S. De Curtis, S. Moretti, and G. M. Pruna, Exploring Drell-Yan signals from the 4D composite Higgs model at the LHC, *J. High Energy Phys.* **04** (2013) 152; D. Barducci, L. Fedeli, S. Moretti, S. De Curtis, and G. M. Pruna, Leptonic final states from di-boson production at the LHC in the 4-dimensional composite Higgs model, *J. High Energy Phys.* **04** (2013) 038.
- [16] G. Aad *et al.* (ATLAS Collaboration), Search for high-mass dilepton resonances in pp collisions at  $\sqrt{s}$  with the ATLAS detector, *Phys. Rev. D* **90**, 052005 (2014); V. Khachatryan *et al.* (CMS Collaboration), Search for physics beyond the standard model in dilepton mass spectra in proton-proton collisions at  $\sqrt{s} = 8$  TeV, *J. High Energy Phys.* **04** (2015) 025.
- [17] G. Aad *et al.* (ATLAS Collaboration), Search for WZ resonances in the fully leptonic channel using pp collisions at  $\sqrt{s} = 8$  TeV with the ATLAS detector, *Phys. Lett. B* **737**, 223 (2014); V. Khachatryan *et al.* (CMS Collaboration), Search for new resonances decaying via WZ to leptons in proton-proton collisions at  $\sqrt{s} = 8$  TeV, *Phys. Lett. B* **740**, 83 (2015).
- [18] A. Thamm, R. Torre, and A. Wulzer, Future tests of Higgs compositeness: direct vs indirect, [arXiv:1502.01701](https://arxiv.org/abs/1502.01701).
- [19] S. De Curtis, M. Redi, and A. Tesi, The 4D composite Higgs, *J. High Energy Phys.* **04** (2012) 042.
- [20] S. De Curtis, M. Redi, and E. Vigiani, Nonminimal terms in composite Higgs models and in QCD, *J. High Energy Phys.* **06** (2014) 071.
- [21] H. Cai, Vector-like Fermions in a minimal composite Higgs model, [arXiv:1405.7664](https://arxiv.org/abs/1405.7664).
- [22] K. Kawarabayashi and M. Suzuki, Partially conserved g vector current and the decays of vector mesons, *Phys. Rev. Lett.* **16**, 255 (1966); Riazuddin and Fayyazuddin, Algebra of current components and decay widths of rho and  $K^*$  mesons, *Phys. Rev.* **147**, 1071 (1966); L. v. Dung and T. N. Truong, Equivalence between vector meson dominance and unitarized chiral perturbation theory, [arXiv:hep-ph/9607378](https://arxiv.org/abs/hep-ph/9607378).
- [23] R. Contino, C. Grojean, D. Pappadopulo, R. Rattazzi, and A. Thamm, Strong Higgs interactions at a linear collider, *J. High Energy Phys.* **02** (2014) 006.
- [24] A. E. Carcamo Hernandez and R. Torre, A composite' scalar-vector system at the LHC, *Nucl. Phys.* **B841**, 188 (2010).
- [25] C. Becchi, A. Rouet, and R. Stora, The abelian Higgs Kibble model, unitarity of the S-operator, *Phys. Lett.* **52B**, 344 (1974); Renormalization of the abelian Higgs-Kibble model, *Commun. Math. Phys.* **42**, 127 (1975); Renormalization of gauge theories, *Ann. Phys. (N.Y.)* **98**, 287 (1976); I. V. Tyutin, Gauge invariance in field theory and statistical physics in operator formalism, [arXiv:0812.0580](https://arxiv.org/abs/0812.0580).
- [26] R. Alonso, M. B. Gavela, L. Merlo, S. Rigolin, and J. Yepes, 'The effective chiral Lagrangian for a light dynamical Higgs,' *Phys. Lett. B* **722**, 330 (2013).
- [27] A. Pich, I. Rosell, and J. J. Sanz-Cillero, Strongly coupled models with a Higgs-like boson, *EPJ Web Conf.* **60**, 19009 (2013).
- [28] C. Degrande, N. Greiner, W. Kilian, O. Mattelaer, H. Mebane, T. Stelzer, S. Willenbrock, and C. Zhang, Effective field theory: A modern approach to anomalous couplings, *Ann. Phys. (N.Y.)* **335**, 21 (2013).
- [29] G. Buchalla, O. Cata, and C. Krause, Complete electroweak chiral Lagrangian with a light Higgs at NLO, *Nucl. Phys.* **B880**, 552 (2014); G. Buchalla and O. Cata, Effective theory

- of a dynamically broken electroweak standard model at NLO, *J. High Energy Phys.* **07** (2012) 101.
- [30] R. L. Delgado, A. Dobado, and F. J. Llanes-Estrada, One-loop  $W_L W_L$  and  $Z_L Z_L$  scattering from the electroweak chiral Lagrangian with a light Higgs-like scalar, *J. High Energy Phys.* **02** (2014) 121; A. Dobado, R. L. Delgado, and F. J. Llanes-Estrada, Strongly interacting electroweak symmetry breaking sector with a Higgs-like light scalar, Proceedings of the II Russian-Spanish Congress “Particle and Nuclear Physics at all Scales and Cosmology” Institute of Cosmos Sciences, Saint-Petersburg, 2013, *AIP Conf. Proc.* **1606**, 151 (2014).
- [31] Fits of precision EW observables lead to more stringent bounds on  $a$  and thus on  $K_1$  but they depend on unknown high-energy effects in virtual states, so they are not as reliable as direct LHC bounds. See M. Baak, J. Haller, A. Hoecker, D. Kennedy, R. Kogler, K. Mönig, M. Schott, and J. Stelzer, The electroweak fit of the standard model after the discovery of a new boson at the LHC, *Eur. Phys. J. C* **72**, 2205 (2012).
- [32] S. Catrchyan *et al.* (CMS Collaboration), Precise determination of the mass of the Higgs boson and tests of compatibility of its couplings with the standard model predictions using proton collisions at 7 and 8 TeV, [arXiv:1412.8662](https://arxiv.org/abs/1412.8662). [See Fig. 9 and Table 12 for the global analysis, Fig. 10 for the direct measurement  $h \rightarrow VV$  (off-shell). See also the last rows of Table 12].
- [33] D. Espriu and F. Mescia, Unitarity and causality constraints in composite Higgs models, *Phys. Rev. D* **90**, 015035 (2014).
- [34] E. P. Wigner, Resonance reactions and anomalous scattering, *Phys. Rev.* **70**, 15 (1946); E. P. Wigner and L. Eisenbud, Higher angular momenta and long range interaction in resonance reactions, *Phys. Rev.* **72**, 29 (1947).
- [35] A. Alboteanu, W. Kilian, and J. Reuter, Resonances and unitarity in weak boson scattering at the LHC, *J. High Energy Phys.* **11** (2008) 010.
- [36] W. Kilian, T. Ohl, J. Reuter, and M. Sekulla, High-energy vector boson scattering after the Higgs discovery, [arXiv:1408.6207](https://arxiv.org/abs/1408.6207).
- [37] J. A. Oller and E. Oset, Two meson scattering amplitudes and their resonances from chiral symmetry and the N/D method, *Nucl. Phys.* **A663**, 629 (2000).
- [38] A. Gomez Nicola and J. R. Pelaez, Meson meson scattering within one loop chiral perturbation theory and its unitarization, *Phys. Rev. D* **65**, 054009 (2002); A. Dobado, M. J. Herrero, and T. N. Truong, Unitarized chiral perturbation theory for elastic pion-pion scattering, *Phys. Lett. B* **235**, 134 (1990); A. Dobado, M. J. Herrero, and T. N. Truong, Study of the strongly interacting Higgs sector, *Phys. Lett. B* **235**, 129 (1990).
- [39] B. Ananthanarayan, G. Colangelo, J. Gasser, and H. Leutwyler, Roy equation analysis of pi pi scattering, *Phys. Rep.* **353**, 207 (2001).
- [40] R. Kaminski, J. R. Pelaez, and F. J. Yndurain, The pion-pion scattering amplitude. III. Improving the analysis with forward dispersion relations and Roy equations, *Phys. Rev. D* **77**, 054015 (2008).
- [41] H. Cai, Higgs decay into a diphoton in the composite Higgs model, *Phys. Rev. D* **88**, 035018 (2013).
- [42] S. Ceci, M. Korolija, and B. Zauner, Model-Independent Extraction of the Pole and Breit-Wigner Resonance Parameters, *Phys. Rev. Lett.* **111**, 112004 (2013).